

Full length article

Tectono-thermal evolution of the Kanggur-Huangshan shear zone, Chinese Tianshan: Insights from integrated geochronology and thermochronology



Meng Luo ^{a,b}, Zhiyuan He ^{c,d}, Fujun Wang ^{a,d}, Yueqiao Zhang ^a, Jianzhang Pang ^e, Ying Wang ^e, Ying Wu ^e, Bihai Zheng ^a, Johan De Grave ^c, Wenbin Zhu ^{a,*}

^a State Key Laboratory for Mineral Deposits Research, Institute of Continental Geodynamics, School of Earth Sciences and Engineering, Nanjing University, Nanjing 210023, China

^b School of Civil Engineering, Wanjiang University of Technology, Ma'anshan, 243031, China

^c Laboratory for Mineralogy and Petrology, Department of Geology, Ghent University, Krijgslaan 281 S8, 9000 Ghent, Belgium

^d Institute of Geosciences, University of Potsdam, Potsdam-Golm, Germany

^e State Key Laboratory of Earthquake Dynamics, Institute of Geology, China Earthquake Administration, Beijing, China

ARTICLE INFO

Keywords:

Tianshan orogenic belt
Kanggur-Huangshan shear zone
(U-Th)/He thermochronology
Apatite fission track dating
Exhumation and cooling
Intracontinental deformation

ABSTRACT

Integrated geo-thermochronometry with structural analysis provide insights into the deformation and exhumation processes within the Kanggur-Huangshan shear zone (KHSZ), a significant transcurrent strike-slip fault and metallogenic belt in the Eastern Tianshan orogenic belt (Central Asia). Previous studies have primarily focused on structural, geochronological and geochemical aspects, often overlooking the exhumation dynamics. This study employs zircon U-Pb, (U-Th)/He (ZHe), apatite fission track (AFT) and (U-Th)/He (AHe) dating alongside field observations and microstructural analysis to elucidate the unroofing processes in the western KHSZ. New zircon U-Pb ages ranging from 280 to 260 Ma and U-Th/He age between 215 and 180 Ma for synkinematic rock, combined with published Ar/Ar data, indicate rapid post-magmatic cooling and shearing in an extensional setting. Subsequently, the region underwent tectonic inversion to transpression and exhumation, with blocks inside the shear zone experiencing more exhumation and forming the positive-flower structures until ca. 200 Ma. Late Jurassic to earliest Cretaceous AFT ages (165–145 Ma) and overlapping AHe ages (155–145 Ma) suggest rapid cooling after differential Jurassic burial, followed by a gradual exhumation of the samples to near-surface levels. A synthesis of existing data indicates that moderate Mesozoic cooling, coupled with Jurassic reburial and Cretaceous-Cenozoic tectonic quiescence, is characteristic of the western KHSZ. This geological history is crucial for understanding the preservation of porphyry Cu deposits as well as epithermal gold and Fe-Cu deposits in the region.

1. Introduction

Shear zones are fundamental components of the Earth's crust, accommodating strain during tectonic events and serving as major conduits for magma and hydrothermal fluid migration. They exhibit transitions between brittle, brittle-ductile, and ductile deformation regimes, providing valuable insights into the mechanical behavior of the lithosphere (Oriolo et al., 2018; Ribeiro et al., 2020). The deformation history recorded in shear zones is complex tied to their exhumation processes, which govern how deeply buried rocks are brought to the surface over geological time. The thermal fluctuations associated with exhumation imprint distinct isotopic signatures on minerals, enabling

researchers to reconstruct deformation histories through geothermochronological methods (Ault et al., 2019). Moreover, shear zones play a critical role in the formation, preservation, and destruction of mineral deposits. Their structural weaknesses and permeability make them ideal pathways for mineralizing fluids, facilitating ore formation in different tectonic settings (Zhai et al., 2000; Groves et al., 2005). However, subsequent deformation and exhumation processes can either preserve or modify these deposits. Burial beneath thick sedimentary cover or in deep crustal settings may provide favorable conditions for long-term preservation, while rapid unroofing can expose deposits to surface weathering and erosion. Additionally, later-stage reactivation of shear zones can lead to remobilization or even destruction of pre-

* Corresponding author.

E-mail address: zwb@nju.edu.cn (W. Zhu).

existing mineralization, redistributing ore-bearing phases along new structural pathways. Understanding the thermal and deformational evolution of shear zones is therefore crucial not only for advancing tectonic models but also for assessing how exhumation histories influence the preservation and economic viability of mineral deposits. Despite their significance, the interplay between exhumation, deformation, and mineral preservation in shear zones remains insufficiently understood, especially in complex orogenic settings where multiple tectonic events overlap.

The Kanggur-Huangshan shear zone (KHSZ) in the southern Central Asian Orogenic Belt (CAOB) provides an ideal setting to investigate these processes (Wang et al., 2008; Muhtar et al., 2022). As one of the largest accretionary orogens in the world, the CAOB records a prolonged history of tectonic activity associated with the subduction and closure of the Paleo-Asian Ocean (Xiao et al., 2003, 2020; Windley et al., 2007). The KHSZ is a prominent transcurrent fault system within this belt, characterized by a complex deformation history (ca. 280–250 Ma) and extensive polymetallic mineralization. Its tectonic evolution has attracted significant attention, with previous studies focusing primarily on its role in Paleozoic subduction-accretion processes and associated mineral deposits (Wu et al., 2017; Muhtar et al., 2022). High-temperature geochronological methods, such as U-Pb and Ar/Ar dating, have been extensively applied to constrain magmatic and metamorphic events, while micro-structural studies have provided insights into the kinematics of deformation (Liu et al., 2016; Han et al., 2018; Deng et al., 2020). However, the Mesozoic and Cenozoic evolution of the KHSZ remains poorly understood, with significant ambiguities surrounding the timing, rates, and spatial patterns of exhumation. Competing models propose varying scenarios for the timing and nature of deformation, reflecting discrepancies in interpretations of structural, petrological, and geochronological datasets (Xu et al., 2003; Qin et al., 2011; Branquet et al., 2012; Wang et al., 2014; Hu et al., 2022; Mao et al., 2022a). Furthermore, previous studies have predominantly focused on high-temperature geochronology, leaving a gap in our understanding of the low-temperature thermal history that records the later stages of exhumation and deformation.

Low-temperature thermochronology, including techniques such as fission-track and (U-Th)/He dating, is particularly effective in capturing exhumation processes within the 60 °C to 240 °C range (Gleadlow et al., 2002a, 2002b; Ehlers and Farley, 2003; Reiners et al., 2004). Despite its potential, thermochronological studies in the KHSZ have been limited and often concentrate on ore bodies rather than wall rocks (Sun et al., 2021). This focus creates potential biases, as exhumation patterns can vary significantly between localized ore systems and the surrounding crust. Such discrepancies underscore the importance of integrating thermochronological data from broader spatial scales to build a more comprehensive understanding of regional tectonic evolution.

This study addresses these gaps by combining multi-system thermochronology with structural and micro-structural analyses to investigate the evolution of the KHSZ. Our research focuses on the syn-kinematic Qiziltag intrusion, a key feature of the western KHSZ, to constrain the timing of deformation and its tectonic implications. Zircon U-Pb and (U-Th)/He, as well as apatite fission track and (U-Th)/He data, are integrated to reconstruct the exhumation history and reveal spatial variations in thermal histories along the shear zone. Field observations and micro-structural analysis complement these datasets, providing critical constraints on deformation mechanisms and the transitions between ductile and brittle regimes. The findings presented here have significant implications for understanding the late-stage evolution of the KHSZ, particularly in relation to Mesozoic-Cenozoic deformation. By synthesizing these results with previous studies, we aim to refine tectonic models of the CAOB and elucidate the processes that govern mineralization and preservation within shear zones (Zhang et al., 2020a; Reinoso et al., 2024). This research not only advances the understanding of the KHSZ but also offers broader insights into the dynamic interplay between deformation, exhumation, and mineralization in complex

orogenic systems.

2. Geological setting

2.1. Regional geology

The Central Asian Orogenic Belt (CAOB) is a vast tectonic complex, bounded by the Siberian craton to the north and the Tarim-North China cratons to the south (Fig. 1a; Sengör et al., 1993), and it records multiple tectono-thermal events over geological time (Dumitru et al., 2001; Windley et al., 2007; Xiao et al., 2013). Initiating in the Neoproterozoic, the CAOB evolved through the amalgamation of continental blocks, volcanic arcs, and accretionary complexes during the Paleozoic. Subsequent intracontinental deformation was largely influenced by several large-scale strike-slip movements, and distant effects related to the complex tectonics along the former Eurasian margin (Hendrix et al., 1992; Xiao et al., 2004; Windley et al., 2007; Jolivet et al., 2010; Nachtergaele et al., 2018; He et al., 2021a). One of the major components of the CAOB is the Tianshan orogenic belt, which extends over 2400 km from the Aral Sea in Uzbekistan to Xinjiang, China. The Chinese segment of the Tianshan is subdivided into Western and Eastern Tianshan along the Urumqi-Korla Road, around 88°E longitude. Eastern Tianshan is further divided into the North, Central, and South Tianshan blocks based on major strike-slip shear zones and variations in basement composition and tectonic settings (Charvet et al., 2007; Gao et al., 2011; He et al., 2021a).

The North Tianshan block, comprising several distinct tectonic units, is structurally segmented by major faults such as the Qincheng, Kangguer, Yamansu, and Aqikekuduke-Shaquanzi faults. These units, from north to south, include the Bogeda-Harlik belt, the Dananhu-Tousuquan arc, and the Aqishan-Yamansu belt. The Bogeda-Harlik belt primarily consists of Ordovician-Carboniferous volcanic rocks, granites and mafic-ultramafic complexes (Fig. 1b; Cunningham et al., 2003; Chen et al., 2011). The Dananhu-Tousuquan arc, a result of subduction-related processes, remains controversial in terms of tectonic models. Some studies attribute to the south-ward subduction of the Junggar oceanic plate (e.g., Zhang et al., 2016), while others suggest northward subduction of the Kangguer oceanic plate (Huang et al., 2018; Zhang et al., 2018), or both (Xiao et al., 2004; Gong et al., 2023). These subduction events gave rise to widespread Ordovician to Permian volcanic and sedimentary sequences, calc-alkaline andesite, and granitoids, which are associated with significant mineralization, including porphyry copper (e.g., the Yuhai-Sanchakou, Yudai, Fuxing and Tuwu-Yandong) and volcanogenic massive sulfide deposits (e.g., the Honghai and Xiaorequanzi) (Du et al., 2018; Mao et al., 2022b). The KHSZ separates the Dananhu-Tousuquan arc from the Aqishan-Yamansu belt, which contains Carboniferous volcanic-sedimentary sequences and numerous iron and iron-copper deposits (Zhang et al., 2020b).

The Central Tianshan block comprises an amphibolite-facies Precambrian crystalline basement overlain by early Paleozoic volcano-sedimentary rocks and intruded by Paleozoic to early Mesozoic plutons (BGMRX, 1993; Hu et al., 2007; Mao et al., 2021). This block is known for hosting sediment-hosted Pb-Zn (–Ag) deposits, such as those found at Caixiasan, Hongyuan, and Yuxi (Zhang et al., 2015). The South Tianshan (often referred to as the Beishan belt in its eastern part) is bounded to the north by the Kawabulak-Xingxingxia fault. A defining characteristic of this region is the occurrence of Silurian-Devonian ophiolitic mélanges along its southern margin, interpreted as either nappes thrust from the north (Han et al., 2011; Xiao et al., 2013) or remnants of back-arc basins (Wang et al., 2018; Zhong et al., 2019).

Although the modern topography of the Tianshan is largely attributed to Cenozoic deformation related to the India-Asia collision (e.g., Molnar and Tapponnier, 1975; Sobel et al., 2006), recent research has revealed that many parts of Central Asia were subject to significant Paleozoic and Mesozoic intracontinental deformation (Jolivet et al., 2010; Glorie and De Grave, 2016; Gillespie et al., 2020; He et al.,

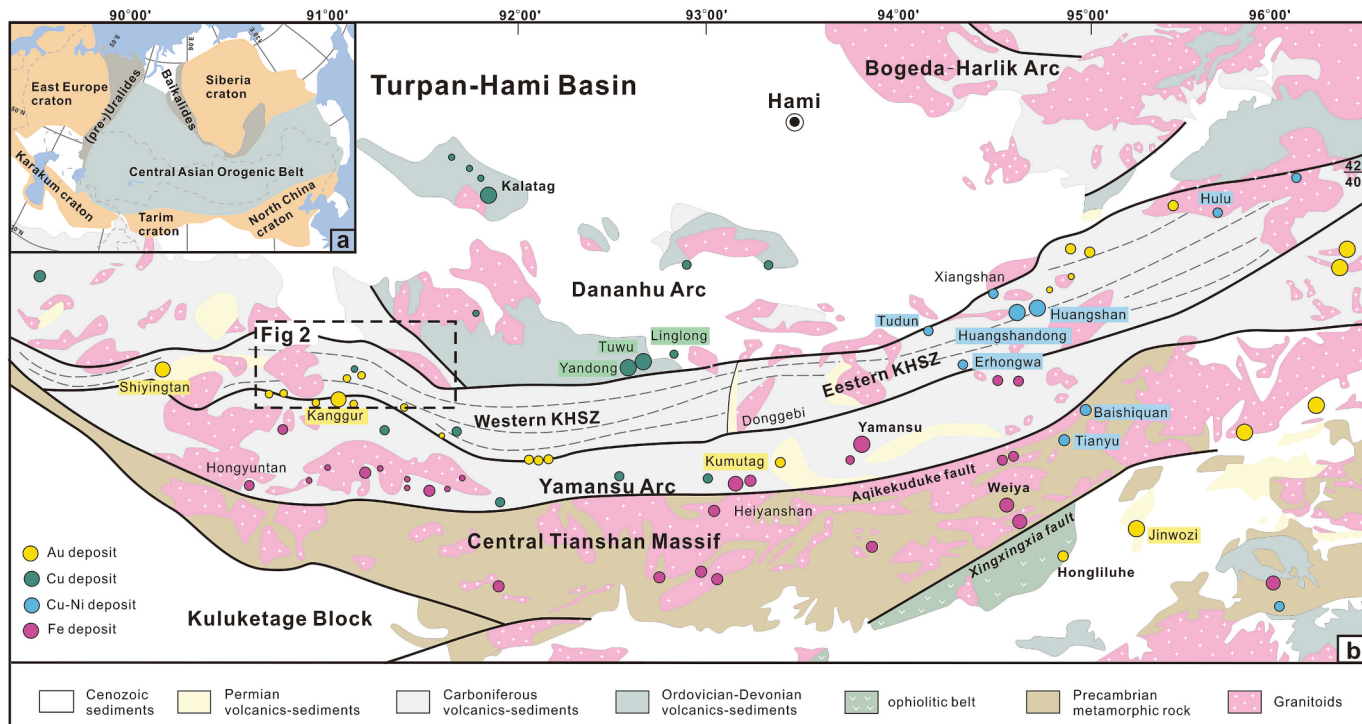


Fig. 1. (a) Simplified tectonic map of the Central Asian Orogenic Belt (CAOB), modified from Sengör et al. (1993). (b) Geological map of the Eastern Tianshan highlighting the study area and distribution of ore deposits (modified from Mao et al., 2019).

2022a). Variations in elevation and exhumation ages over short distances suggest a complex history of tectonic reactivation and erosion, with buried structures accommodating contrasting exhumation histories (e.g., Hendrix et al., 1992; Glorie and De Grave, 2016; He et al., 2021b, 2022b; Yin et al., 2023).

2.2. Structural features of the Kanggur-Huangshan shear zone

The Kanggur-Huangshan shear zone (KHSZ) extends over 500 km in length and varies between 10 and 30 km in width (Fig. 1b). It is predominantly composed of strongly deformed Carboniferous sedimentary-volcanic rocks, which have undergone significant metamorphism, resulting in the formation of dark schists and meta-conglomerates (Wang et al., 2014; Hu et al., 2022). These schist/ meta-sedimentary rocks exhibit a well-developed penetrative foliation, characterized by the preferred alignment of metamorphic mica, calcite, and quartz, along with associated mineral lineations. The foliation strikes ENE to ESE and dips between 65° and 90° to the north or south, paralleling the boundaries of the shear zone. The granitic rocks within the KHSZ can be classified into two main groups: (1) the strongly deformed Carboniferous arc-related granite, which dates to ~ 330–300 Ma (Zhou et al., 2010); and (2) syn-kinematic granite formed between ca. 290 and 230 Ma (Branquet et al., 2012; Wang et al., 2014; Muhtar et al., 2019, 2022; Hu et al., 2022; Mao et al., 2022a).

The current structural configuration of the KHSZ is characterized by an asymmetric positive style, with a narrower northern section and a broader southern section (BGMRX, 1993; Xu et al., 2003; Zhang et al., 2014). Various models have been proposed to explain the internal structural deformation of the Kanggur tectonic belt. These include: (1) coaxial N-S compression (Xu et al., 2003); (2) a combination of N-S compression and dextral shear leading to the latest brittle-ductile deformation (Wang et al., 2019); (3) early N-S compression followed by superimposed dextral shearing (Wang and Shu, 1997; Wang et al., 2014); and (4) a transition from sinistral transtension to dextral motion and compression (Mao et al., 2022a). Despite these insights, the timing and mechanisms underlying the shearing processes remain uncertain.

The Kanggur-Huangshan tectonic belt also exhibits notable differences in metamorphism and deformation between its eastern and western segments. The western part (Kanggur) demonstrates brittle-ductile deformation (Fig. 1b and 2), featured by a typical metamorphic mineral assemblage that includes actinolite, biotite, and chlorite, indicative of lower greenschist facies conditions (Xu et al., 2003; Wang et al., 2014). In contrast, the eastern segment (Huangshan-Jingerquan) displays a mineral assemblage of kyanite, staurolite, and sillimanite, suggesting metamorphic conditions within the greenschist to amphibolite facies (Wang et al., 1994; Xu et al., 2003; Branquet et al., 2012; Mao et al., 2022b). Accompanying these different metamorphic conditions, the distribution of mineral deposits also varies. Gold deposits are predominantly found in the western part of the shear zone (e.g., the Kanggur, Hongshi, and Shiyington) (Fig. 1b; Sun et al., 2015; Wang et al., 2016; Muhtar et al., 2021), while magmatic Ni-Cu sulfide deposits are more prevalent in the eastern segments (e.g., the Huangshan and Huangshandong) (Wu et al., 2017; Han et al., 2018).

2.3. Geology of the intrusions

The Qiziltag pluton, also referred to as the Jueluotag pluton, is situated along the northern margin of the Dacaotan fault. This tongue-shaped pluton spans ~ 30 km in length, exhibiting a wider eastern end that narrows towards the west (Fig. 2). The presence of wrench features and a parallel tail to the main foliation indicates syn-kinematic mega-fabrics consistent with dextral kinematics (Wang et al., 2014). Surrounding this batholith, Carboniferous rocks display contact metamorphism, characterized by andalusite and/or pyrophyllite-bearing black schist. The mylonitic foliation in this area is generally subvertical and oriented nearly E-W (Fig. 3a). The Qiziltag granitic pluton exhibits either homogeneous or porphyritic textures, with a gradual lithological transition from earlier gneissic biotite granite to later bimodal intrusions, with age from 289 to 271 Ma (Li et al., 2006; Muhtar et al., 2019). Samples collected from various locations within the pluton yield hornblende $^{40}\text{Ar}/^{39}\text{Ar}$ plateau ages ranging from 277 to 272 Ma, biotite ages from 261 to 254 Ma, and K-feldspar ages from 240 to 220 Ma.

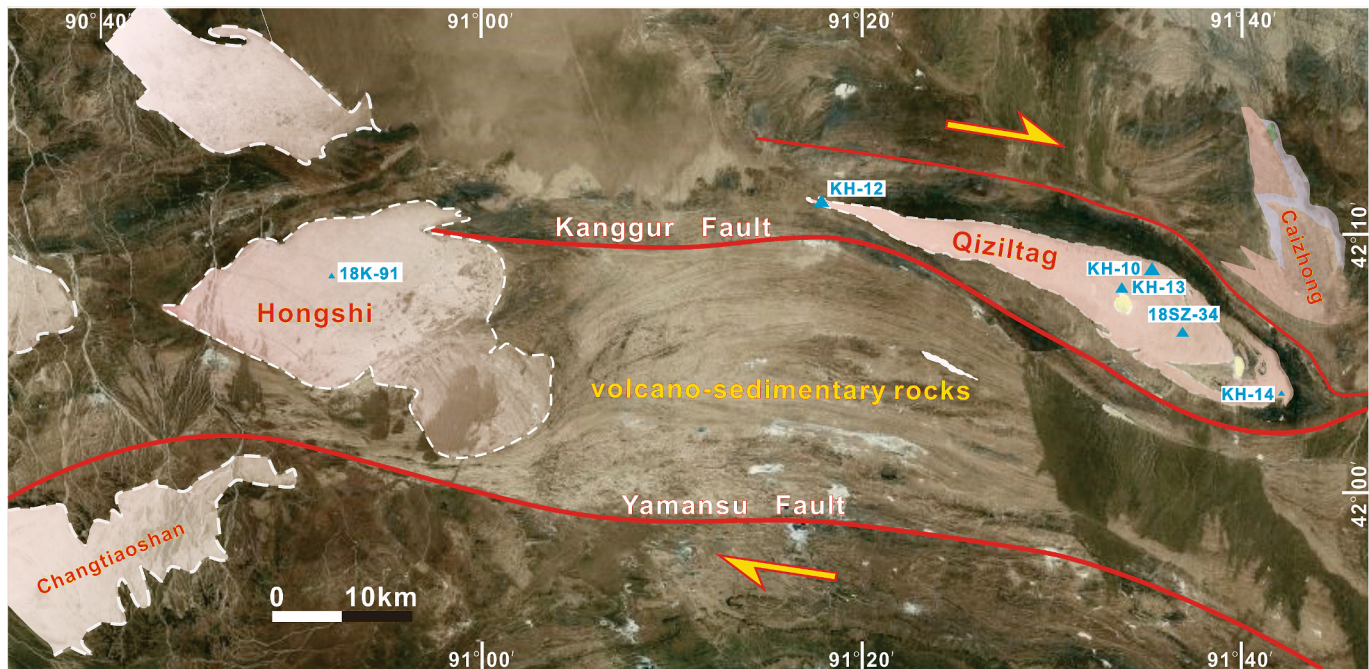


Fig. 2. Satellite image of the Qiziltag and Hongshi plutons from Google EarthTM, showing sample locations.

(Wang et al., 2008) (Table 1). The adjacent Hongshi pluton (Fig. 2), featured by porphyritic granite, has a zircon U-Pb age 282 ~ 273 Ma (Zhou et al., 2010; Muhtar et al., 2022) and intruded into the lower Carboniferous Yamansu Formation. This granitic pluton displays typical brittle deformation features, exhibiting a domino structure that indicates a dextral sense of shearing and clockwise rotation.

3. Sample description and analytical techniques

Samples were collected from locations shown in Fig. 2. Structural observations and chronological analyses of the granitic plutons are conducted to assess the conditions under which deformation took place. Additionally, thermochronological analysis of five samples from both sides of the Kanggur fault was performed to evaluate cooling and unroofing associated with discrete fault block development and exhumation in the western part of the KHSZ.

Previous studies have indicated that deformation predominantly occurred along the margins of the pluton and surrounding country rocks. It is noted that the northern side of the intrusion exhibited distinct subhorizontal lineations (Fig. 3a). Micro-structures resulting from moderate to high-temperature sub-solidus deformation are easily observable in the Qiziltag samples. These include quartz-filled fractures in feldspar phenocrysts, stretching of the feldspar, and the presence of wavy, flame-like lamellae of perthite (Fig. 3b-d). Such features, described by Passchier and Trouw (2005) for the submagmatic stage of granites, suggest the involvement of a residual melt during the plastic deformation of feldspar (Vernon, 2004).

3.1. Zircon U-Pb dating

Zircon U-Pb dating was performed using laser ablation inductively coupled plasma mass spectrometry (LA-ICP-MS) at Nanjing Hongchuang Geological Exploration Technology Service Co., Ltd. The analytical setup included a Resolution SE model laser ablation system (Applied Spectra, USA) equipped with an ATL (ATLEX 300) excimer laser and a Two Volume S155 ablation cell. Analyses were conducted using a 30 μm diameter spot at a frequency of 5 Hz and a fluence of 2 J/cm². Zircon 91,500 served as the primary reference material, analyzed twice, while GJ-1 was used as a secondary reference material, analyzed once every

10–12 sample analyses. Data reduction was performed using the Iolite software package (Paton et al., 2010).

3.2. Thermochronological analysis

(U-Th)/He analysis was conducted at the State Key Laboratory of Earthquake Dynamics, China Earthquake Administration. Euhedral crystals, free of impurities and internal fractures, were handpicked under polarized light, with their size measured for alpha ejection correction (Farley et al., 1996). Apatite and zircon crystals were loaded into Pt and Nb tubes, respectively, for measuring He abundances using laser mass spectrometry under vacuum at ~ 1000 °C for 5 min and > 1000 °C for 10 min. U and Th concentrations were determined by isotope dilution using a quadrupole inductively coupled plasma-mass spectrometer. For zircon (U-Th)/He (ZHe) analysis, the Nb tubes containing outgassed crystals were digested in HF for 48 h and HCl for 24 h at ~ 220 °C in a pressure bomb. For apatite (U-Th)/He (AHe) analysis, the Pt tubes containing outgassed crystals were digested in HNO₃ at room temperature. Durango apatite and Fish Canyon Tuff zircon were run as reference standards with each sample batch, and Penglai zircon (Li et al., 2017) was also included as an additional check on analytical accuracy.

For the apatite fission track experiment, grains were embedded in epoxy resin on glass slides, polished to expose internal apatite surfaces, and etched in 5 M HNO₃ at 20 °C for 20 s to reveal the spontaneous fission tracks (Barbarand et al., 2003). Sample preparation and fission track counting were conducted at the State Key Laboratory for Mineral Deposits Research, Nanjing University. Uranium analytical measurements were performed at the State Key Laboratory of Earthquake Dynamics, China Earthquake Administration using a Resolution M50 ArF excimer laser at a wavelength of 193 nm, coupled with an Agilent 7900 quadrupole ICP-MS to determine ion signal intensity. Detailed analytical procedures for fission track chronometry using laser ablation ICP-MS are described in Pang et al. (2017).

3.3. Thermal history modeling

Inverse thermal history models were generated using the QTQt software. This software employs a Bayesian trans-dimensional Markov

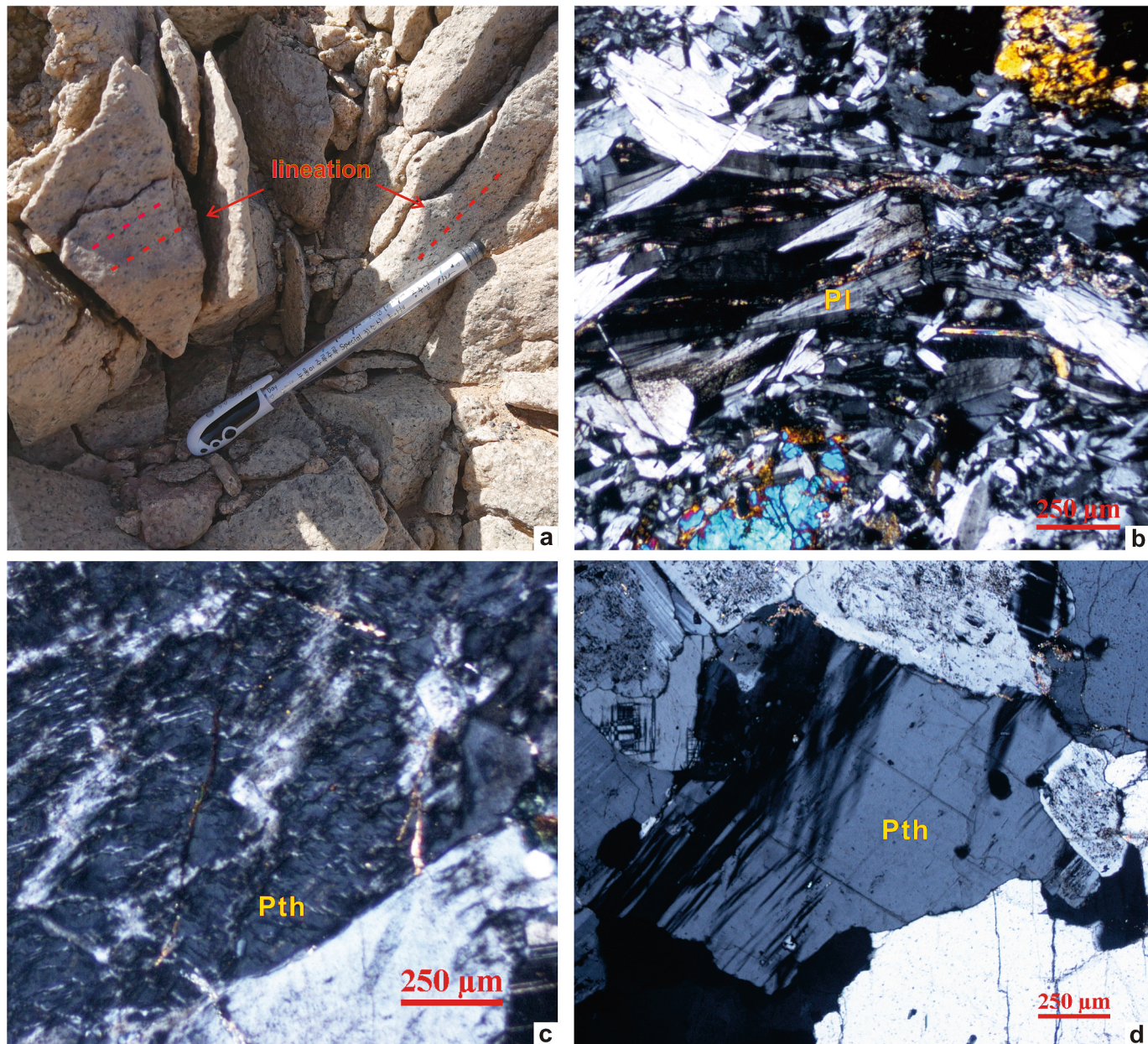


Fig. 3. Photomicrographs illustrating the mineralogy and textural features of representative samples from the Qiziltag pluton: (a) Pluton lineation; (b) Feldspar stretching; (c) Quartz-filled fractures in feldspar phenocrysts; (d) Flame-like lamellae in perthite. Abbreviations: Pl – plagioclase, Pth – perthite.

Chain Monte Carlo approach to invert low-temperature thermochronology data, producing a series of accepted thermal histories based on the data (Gallagher et al., 2009). Within QTQt, AHe and ZHe data can be resampled from their ages, allowing for the accommodation of some undefined uncertainties by considering the He ages as less precise while still honoring the observed ages (Gallagher, 2012). For modeling, the multikinetic annealing model was applied to projected AFT lengths using D_{par} as a kinetic parameter (Ketcham et al., 2007), the damage-diffusion model of Flowers et al. (2009) for AHe data, and the zircon radiation damage accumulation and annealing model for ZHe data (Guenther et al., 2013).

4. Results

4.1. Zircon U-Pb dating results

Zircon U-Pb dating was conducted on four granitic rock samples from

the Qiziltag pluton, with the results in Supplementary Material Table S1. Cathodoluminescence (CL) images of representative zircon grains are shown in Fig. 4. The zircon grains exhibit oscillatory zoning and lack inherited cores, with high Th/U ratios ranging from 0.1 to 0.4, consistent with a magmatic origin. The samples – KH-10, KH-12, KH-13, and KH-14 – yielded weighted mean $^{206}\text{Pb}/^{238}\text{U}$ ages of 279.4 ± 4.2 Ma ($n = 20$; Fig. 4a), 266.4 ± 9.3 Ma ($n = 19$; Fig. 4b), 280.9 ± 3.7 Ma ($n = 18$; Fig. 4c), and 288.2 ± 4.0 Ma ($n = 20$; Fig. 4d), respectively. As these zircons are magmatic in origin, the dates are interpreted as the time of zircon crystallization. The weighted mean ages of these samples overlap within the margin of error, suggesting that the Qiziltag pluton was emplaced during the late Permian (ca. 288.2–266.4 Ma).

4.2. Apatite fission track dating results

AFT data are summarized in Table 2, with track length histograms and radial plots provided in Fig. 5. All samples passed the chi-square

Table 1

Summary of geochronological and thermochronological data from the western Kanggur-Huangshan shear zone.

Location	Mineral	Dating method	Age (Ma)	Reference
Shiyingtan pluton	Zircon	U-Pb	342.0 ± 11.0	Zhou et al., 2010
	Zircon	U-Th/He	253.7 ± 16.4	Sun et al., 2020
	Apatite	U-Th/He	145.9 ± 9.2	Zhou et al., 2010
	Zircon	U-Pb	284.1 ± 5.8	
Guandao pluton	Zircon	U-Pb	288.9 ± 1.9	Muhtar et al., 2019
	Zircon	U-Pb	291.5 ± 1.7	
	Zircon	U-Pb	287.9 ± 3.1	
	Zircon	U-Pb	278.5 ± 1.8	
	Zircon	U-Pb	278.1 ± 2.3	
	Zircon	U-Pb	271.6 ± 1.6	Li et al., 2006
	Zircon	U-Pb	279.4 ± 4.2	This study
	Hornblende	Ar-Ar	278.4–272.2	Wang et al., 2008
	Biotite		261.0–253.9	
	Feldspar		240.8–226.3	
Hongshi pluton	Zircon	U-Pb	273.6 ± 2.1	Muhtar et al., 2022
	Zircon	U-Pb	282.7 ± 4.2	Zhou et al., 2010
	Zircon	U-Pb	344.2 ± 3.9	Sun et al., 2012
	Zircon	U-Pb	337.6–334.0	Wang et al., 2016
	Sericite	Ar-Ar	262.0 ± 1.0	Sun et al., 2012
	Sericite	Ar-Ar	249.6–248.6	Muhtar et al., 2021
	Zircon	U-Pb	316.0 ± 4.0	Li et al., 2006
	Zircon	U-Pb	267.8 ± 1.6	Ren et al., 2006

test, indicating a single population. Samples from the Qiziltag pluton (18SZ-34, KH-10, and KH-13) yielded indistinguishable younger ages of ~145 Ma, whereas the Hongshi sample (18 K-91) returned an older age of 165 ± 15 Ma. Mean track lengths (MTL) suggest moderate thermal disturbance, with values ranging from 12.4 to 13.2 μm. The length-frequency distributions are asymmetrical and relatively broad (Green et al., 1986), with σ-values (standard deviation) of ~1.3 μm, and exhibit negative skewness (Fig. 5a'-c'). These track length data indicate that the samples passed through the apatite partial annealing zone (APAZ; 120–60 °C) at a moderate rate, resulting in noticeable track shortening.

4.3. (U-Th)/He dating results

The AHe ages for eight single grains from two samples are presented in Table 3. These ages exhibit a relatively narrow range of effective uranium (eU) concentrations and grain size (Rs). Sample KH-10 yielded young and consistent AHe ages, with a weighted mean age of 145.6 ± 3.8 Ma and standard deviations below 20 %. In contrast, the individual AHe ages for sample KH-13 ranged from 147.7 ± 3.4 Ma to 159.6 ± 4.2 Ma, with a slight negative trend between age and Rs (Fig. 6b). The overlap of AHe ages with AFT ages may suggest a period of rapid cooling.

The ZHe data for thirteen single grains from four samples displayed considerable inter-sample age dispersion. Consistent with previous research, ZHe age dispersion in slowly cooled rocks is often influenced by radiation damage, grain size, and morphology (Guenther et al., 2014). These relationships can be observed in the age versus Rs and age versus eU plots. For sample KH-14, a negative correlation was observed between ZHe age and eU (Fig. 6c). However, no significant trends were observed for the other samples. Sample KH-13c, with an anomalously

low eU value of 30 ppm (significantly lower than the 400–600 ppm range of other grains), yielded a younger age and was excluded from the mean age calculation. Similarly, for sample KH-10a, a larger eU value was associated with a younger age. Other factors, such as eU zonation, eU-rich micro-inclusions, He implantation, and chemical composition, may also contribute to (U-Th)/He age dispersion, though these factors are more difficult to routinely assess.

4.4. Thermal history modeling results

Thermal history modeling was performed using a time–temperature model, with biotite $^{40}\text{Ar}/^{39}\text{Ar}$ ages (ca. 260 Ma) (Wang et al., 2008) used as the initial temperature constraint. The present-day surface temperature was assumed to be 10°C, with a possible variation of ± 10°C. Although there is no direct evidence of Jurassic reburial in our area, the presence of residual Jurassic strata nearby suggests that the samples may have been buried to some depths after being exposed to near-surface conditions during the Jurassic (Gong et al., 2021). This assumption was incorporated as a prior probability in some models. Given the complexities associated with the (U-Th)/He systematics, less weighting was given to AHe and ZHe data. Initially, AFT data were used to establish a baseline, which was then refined with additional constraints and model iterations. The AFT sample 18 K-91 was excluded from the modeling due to the absence of track length measurements.

The model outputs are shown in Fig. 7. Models incorporating only AFT data (Fig. 7a) revealed similar cooling histories for all samples, characterized by rapid to moderate cooling from 260 Ma (350 °C) to 200 Ma (100 °C), followed by slower cooling (<0.5 °C/Ma). Sample 18SZ-34 exhibited a more subdued cooling rate (<0.2 °C/Ma) as it approached the near surface. In a subsequent model (Fig. 7a'), which incorporated the possibility of Jurassic surface exposure, all samples underwent reburial at approximately 70°C, with sample KH-10 displaying the steepest cooling path. When AHe data were added to the models, the general cooling trends remained unchanged but extended the cooling period from ~200 Ma to ~160 Ma, with narrower 95 % confidence intervals (Fig. 7b). Under the reheat scenario (Fig. 7b'), cooling varied among samples. For instance, sample KH-13 showed cooling to ~50 °C around 200 Ma, followed by slight reburied and subsequent cooling to near-surface conditions around 160 Ma. Meanwhile, sample KH-10 exhibited consistent cooling until 150 Ma. Incorporating ZHe ages further stabilized the trends. With the added data, the thermal history was less influenced by the Jurassic surface exposure constraint (Fig. 7c'). Sample KH-13 experienced moderate cooling (~5 °C/Ma) from 260 Ma to 200 Ma, a minor Jurassic reburial, and further cooling to near-surface conditions. Sample KH-10, on the other hand, maintained a steady cooling rate of ~3 °C/Ma.

5. Discussion

5.1. Mesozoic cooling and deformation: Heterogeneity and regional implications

The controversy over whether Mesozoic cooling and deformation in the Tianshan were continuous or episodic remains unresolved. Hendrix et al. (1992) and Dumitru et al. (2001) proposed three distinct deformation episodes, with slight variations in timing. In contrast, Jolivet et al. (2010) and Glorie et al. (2011) identified four cooling stages. However, sedimentological and thermochronological evidence from the Kyrgyz Tianshan suggests a more prolonged tectonic quiescence during the Mesozoic, with significant uplift and exhumation largely confined to the late Cenozoic (e.g., Bullen et al., 2001; Macaulay et al., 2014). Yin et al. (2023) suggested that discrepancies in deformation timing may stem from sparse and localized datasets in this structurally complex region. The Tianshan, characterized by extensive strike-slip fault systems, is partitioned into fault-bounded tectonic blocks (Charvet et al., 2007; Wang et al., 2008; He et al., 2021a). Major boundary fault zones

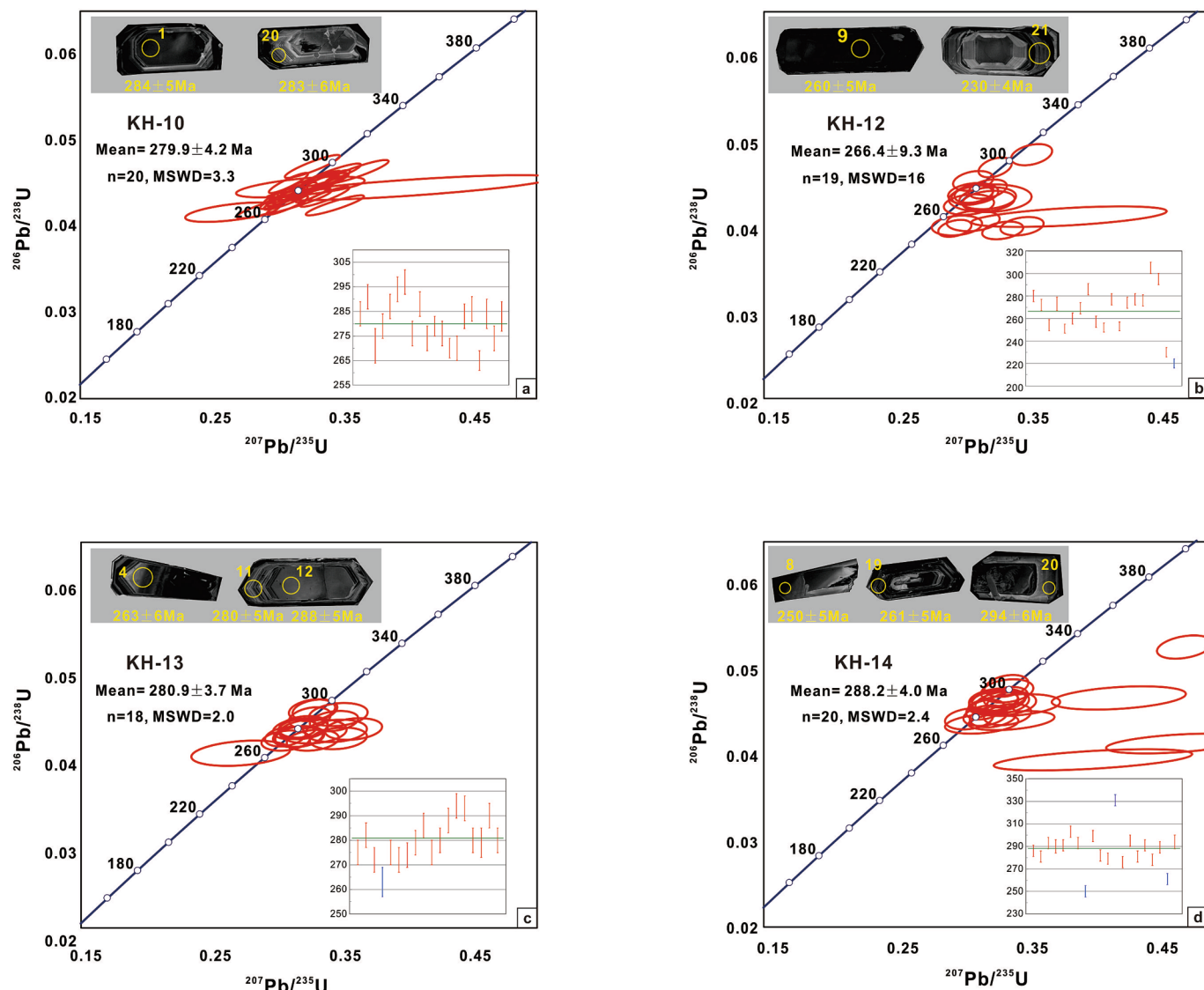


Fig. 4. Zircon U-Pb concordia diagrams and weighted mean ages for granites from the Qiziltag pluton: (a) KH-10; (b) KH-12; (c) KH-13; (d) KH-14. Cathodoluminescence images of representative zircon grains are shown as insets with analytical numbers and spots marked for Hf and age determinations. MSWD – mean square weighted deviation.

Table 2

Apatite fission track data for samples from the western Kangjur-Huangshan shear zone.

Sample No.	No. of grains	N _s	ρ_s (10^5 cm $^{-2}$)	^{238}U (ppm)	D _{par} (μm)	P(χ^2) (%)	Central age (Ma \pm 1 σ)	N _{length}	Mean track length (μm)	Standard Deviation (μm)
18SZ-34	27	162	8.4	11.3	2.0	0.33	148 \pm 12	81	12.4	1.3
KH-10	32	395	8.2	10.0	1.7	0.41	144.9 \pm 11	124	12.5	1.4
KH-13	27	434	9.0	12.2	1.9	0.25	145.6 \pm 8.5	111	13.2	1.3
18 K-91	24	172	10.4	12.7	1.6	0.06	165 \pm 15			

N_s = number of spontaneous tracks counted; ρ_s = spontaneous track density; D_{par} = long axis of track etch pit; P(χ²) = chi-squared probability; N_{length} = the number of lengths measured.

exhibit repeated reactivation and exhumation episodes (e.g., Dumitru et al., 2001; Jolivet et al., 2010; Wang et al., 2018b). Consequently, younger ages are often associated with fault zones, while older ages dominate regions farther away. Deformation also appears temporally and spatially partitioned, a pattern observed in other intracontinental mountain belts such as the Sanjiang orogenic belt (Yunnan) (Akciz et al., 2008; He et al., 2023a).

Our study underscores the value of integrating additional thermo-chronological data to refine exhumation histories (e.g., Glorie et al.,

2019). Using AFT data alone, cooling appeared to culminate by 200 Ma. However, the inclusion of AHe data extended the cooling period to 150 Ma, highlighting cooling heterogeneities across samples. For instance, Sample KH-13 aligns with previous studies reporting deformation during the Permian-Triassic, Triassic-Jurassic, and Late Cretaceous (Hendrix, 2000; Dumitru et al., 2001; Jolivet et al., 2010). In contrast, sample KH-10 reveals a more continuous cooling history, and we propose that Jurassic reburial likely played a role in this divergence, influencing thermal histories and complicating the interpretation of

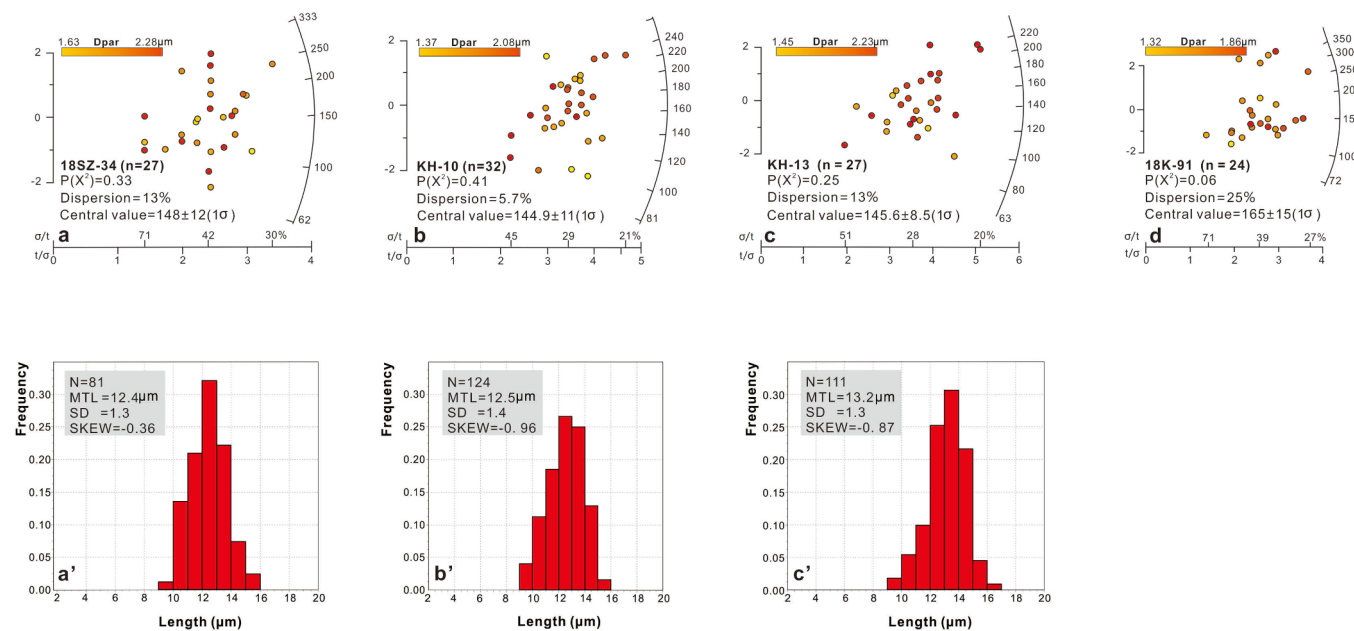


Fig. 5. (a-d) Radial plots of apatite fission-track (AFT) ages for samples constructed using Radial Plotter software (Vermeesch, 2009). Dpar values are indicated using a red/yellow color scale. (a'-c') Frequency plots depicting the distribution of confined fission tracks for corresponding samples. Track length histograms include N (number of spontaneous tracks counted), MTL (mean track length), and SD (standard deviation).

Table 3
Apatite and zircon (U-Th)/He data for samples from the Qiziltag intrusion.

Sample No.	He ncc	U ppm	Th ppm	Th/U	eU ppm	Rs μm	FT	Uncor. Age Ma	Ft-cor. Age Ma	Error ± 1σ Ma	Averate Age Ma	Error ± 1σ Ma	Length μm	Wid-ave μm
Apatite														
KH-10a	0.72	19.29	26.96	1.4	25.63	40.40	0.70	103.92	148.67	3.65			189.43	72.43
KH-10b	0.69	24.44	23.78	0.97	30.02	39.70	0.66	97.18	147.24	3.48			165.39	72.86
KH-10c	0.28	14.66	14.77	1.01	18.14	37.10	0.67	96.83	145.39	4.61			138.39	69.74
KH-10d	0.56	15.9	19.28	1.21	20.43	44.80	0.72	101.82	141.22	3.43			159.33	85.61
											145.63	3.79		
KH-13a	0.75	14.32	18.13	1.30	18.58	47.00	0.75	110.77	147.69	3.36			173.39	88.20
KH-13b	1.20	25.36	31.12	1.26	32.68	43.80	0.73	113.82	156.56	3.52			184.94	80.10
KH-13c	0.59	18.46	20.24	1.12	23.22	39.40	0.70	112.23	159.64	4.20			156.41	73.03
KH-13d	0.76	16.04	23.42	1.50	21.54	44.00	0.73	116.20	158.53	4.23			165.61	82.19
											155.61	3.83		
Sample No.	He ncc	U ppm	Th ppm	Th/U	eU ppm	Rs μm	FT	t Ma	Ft-cor. Ma	Error ± 1σ Ma			Length μm	Wid-ave μm
Zircon														
KH-10a	736.61	1046.02	269.16	0.26	1109.27	90.10	0.87	176.07	202.15	4.58			402.39	127.94
KH-10b	533.44	459.48	132.75	0.30	490.68	100.50	0.88	195.80	221.49	4.88			482.32	150.94
KH-10c	620.12	780.22	227.55	0.30	833.69	93.60	0.88	193.87	221.31	4.92			375.81	138.47
											214.98	4.79		
KH-12a	70.75	847.80	322.06	0.39	923.48	48.40	0.77	141.98	185.35	4.27			200.27	74.52
KH-12b	122.26	797.65	523.34	0.67	920.64	61.80	0.81	135.66	166.86	3.59			218.18	103.12
KH-12c	150.74	1359.38	431.79	0.33	1460.85	53.40	0.79	148.49	188.68	6.04			210.49	83.24
											180.30	4.63		
KH-13a	61.37	433.91	162.23	0.38	472.04	52.90	0.79	165.00	210.19	3.77			245.89	75.21
KH-13b	49.09	405.80	141.79	0.36	439.12	57.10	0.80	135.67	169.59	5.53			214.89	84.21
KH-13c*	3.39	22.94	31.83	1.42	30.42	60.20	0.81	128.39	159.49	2.81			200.62	103.17
KH-13d	128.66	563.24	209.49	0.38	612.47	65.40	0.82	160.71	195.04	3.75			264.42	104.49
											191.60	3.96		
KH-14a	226.20	1056.09	324.44	0.32	1132.33	67.0	0.83	152.33	183.75	3.29			247.05	99.43
KH-14b	188.65	589.07	298.66	0.52	659.25	63.6	0.84	194.42	232.84	4.04			267.94	92.47
KH-14c	163.77	485.96	189.33	0.40	530.45	63.9	0.84	196.82	235.71	4.36			288.36	92.40
											217.43	3.90		

eU—effective U concentration that weighs U and Th for their alpha productivity and is computed as [u] + 0.235*[Th] (Flowers, 2009); Ft—alpha ejection correction (Farley et al., 1996); Rs—half the width of a single grain.* datum identified as an outlier.

thermochronological data. Because in the case of the Tianshan region, the Mesozoic tectonic environment was characterized by a fully intra-continental orogenic setting, with major magmatic activity largely constrained to the Triassic. Jurassic magmatism in this region was

extremely limited. Recent studies (e.g., Wang et al., 2022, Wang et al., 2024) have demonstrated that the sparse Jurassic-Cretaceous igneous rocks in the Tianshan consist primarily of small dikes and minor intrusions, which typically have a localized thermal influence and were

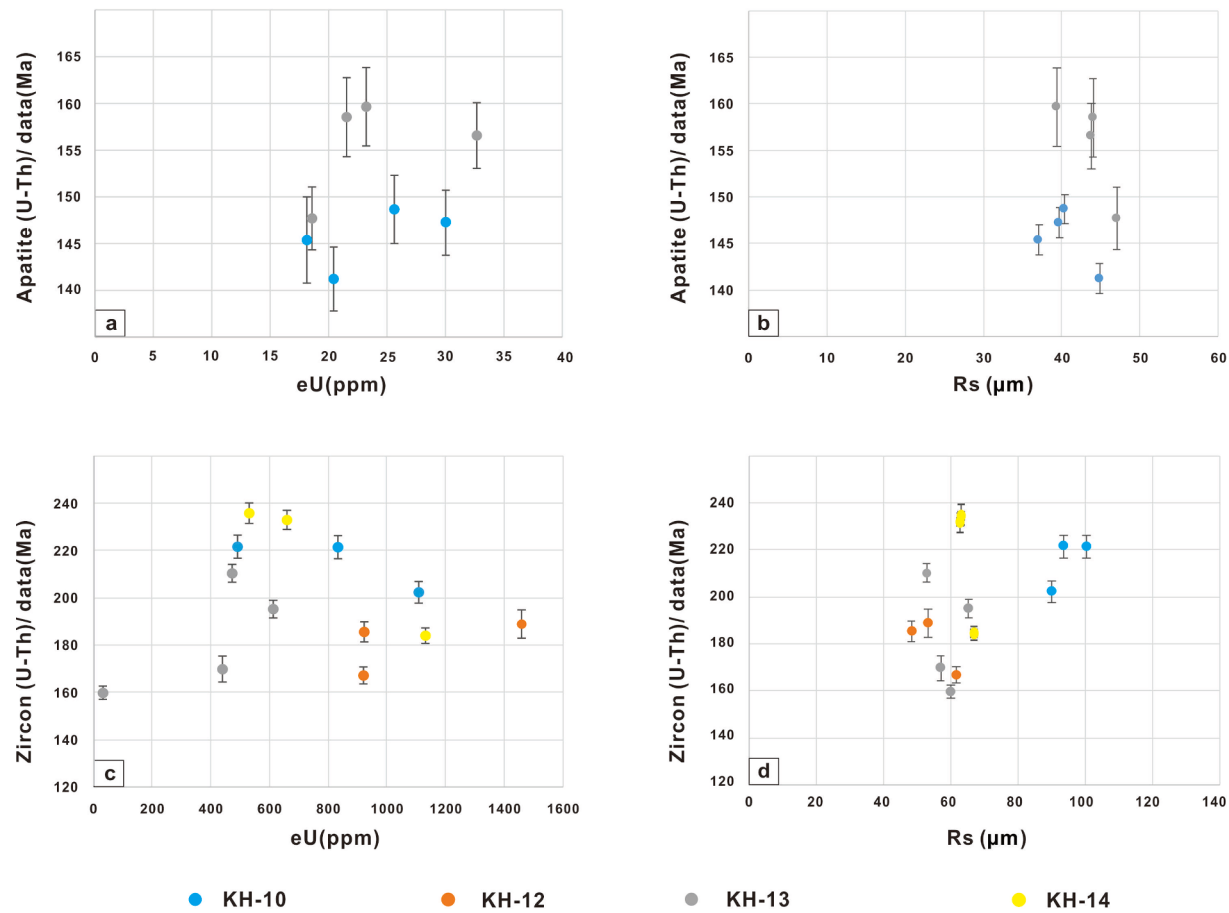


Fig. 6. Relationship between helium (He) ages and: (a) Effective uranium concentration (eU, ppm) for apatite He (AHe); (b) Equivalent spherical radius (Rs) for AHe; (c) eU concentration for zircon He (ZHe); (d) Rs for ZHe. Error bars indicate $\pm 1\sigma$ uncertainties. See text for further discussion.

unlikely to induce large-scale thermal overprinting of the surrounding country rocks. It is noted that rather than being driven by a major tectonic regime shift, Jurassic sedimentation in the Tianshan was primarily controlled by post-orogenic peneplanation, where prolonged surface erosion gradually transported material from elevated regions to lower-lying areas for deposition.

Jurassic reburial is pronounced in some areas but less so in others. In the northern Bogda region, strong Jurassic burial is evident, with single-grain AFT ages from Early Triassic sandstones younger than their depositional ages, indicating significant reburial (He et al., 2023b; Song et al., 2023). Conversely, sedimentological data suggest limited transport distances for Jurassic deposits in areas close to our study region, implying mild reburial (Chen et al., 2011). In the Tuwu-Yandong area, Gong et al. (2021) observed that ore-bearing intrusions were overlain by the Middle Jurassic Xishanyao Formation, with inferred reburial temperatures reaching the upper limit of the APAZ ($\sim 60^\circ\text{C}$). In the Aqishan-Yamansu belt, Jurassic reburial was insufficient to reset AFT ages, despite granites being overlain by Jurassic sandstones (Sun et al., 2021). Our models suggest Jurassic burial temperature of $60\text{--}100^\circ\text{C}$, corresponding to depth of ca. 2 km. This mild burial, while not strongly recorded by thermochronometers, likely influenced cooling rates. Mesozoic cooling rates in the Eastern Tianshan were limited, not exceeding 5°C/Ma (Luo et al., 2023; Chen et al., 2020; Gillespie et al., 2017a; He et al., 2023b; Sun et al., 2021). This may explain why sample KH-10 exhibits similar thermochronological ages without reheating evidence in the thermal model. Within the Tuwu-Yandong area, samples from the same fault zone exhibit varying cooling histories and ages. For instance, Yin et al. (2019) and He et al. (2022a) reported younger AFT ages and continuous cooling until the mid-Cretaceous, while Gong et al.

(2021) suggested an older cooling history, including Jurassic reburial. These discrepancies could result from remnant Mesozoic landforms inherited from Paleozoic orogenic processes, exerting complex control over structural evolution. Local geomorphology, characterized by onlap structures and paleo-relief infilling, likely influenced differential cooling patterns on small spatial scales.

Jurassic exhumation is a well-described phenomenon in some parts of the Tianshan region (Jolivet et al., 2010; De Grave et al., 2014), for example, alluvial fan systems were deposited in response to renewed tectonic activity in several near-Tianshan basins (Sobel, 1999; Yang et al., 2015). In the Beishan area to the south, significant thrusting and nappe emplacement occurred within fold-thrust belts, with minimum displacements of 120–180 km, as indicated by stratigraphic and sedimentological evidence (Zheng et al., 1996; Zhang and Cunningham, 2012; Liu et al., 2023). In addition to the Triassic and Jurassic periods, evidence of Late Cretaceous deformation is also significant (Hendrix, 2000; Dumitru et al., 2001; Jolivet et al., 2010). The intensity of Cretaceous cooling varied spatially, with enhanced cooling in the Eastern Tianshan compared to the western-middle regions. Existing basement rocks low-temperature thermochronology records from the Yili block of the Western Tianshan primarily indicate Triassic-Jurassic cooling and exhumation events. Early Cretaceous cooling has also been documented in regions such as the Nalati and Wusun mountains. However, the overall extent and magnitude of exhumation in the Western Tianshan appear to be lower and less widespread compared to the Eastern Tianshan (e.g., Wang et al., 2018b; He et al., 2022b). The southern border, including the eastern segment of the Central Tianshan and Beishan regions, experienced significant cooling that exposed the deeper basement (Gillespie et al., 2017b; He et al., 2022a; Luo et al.,

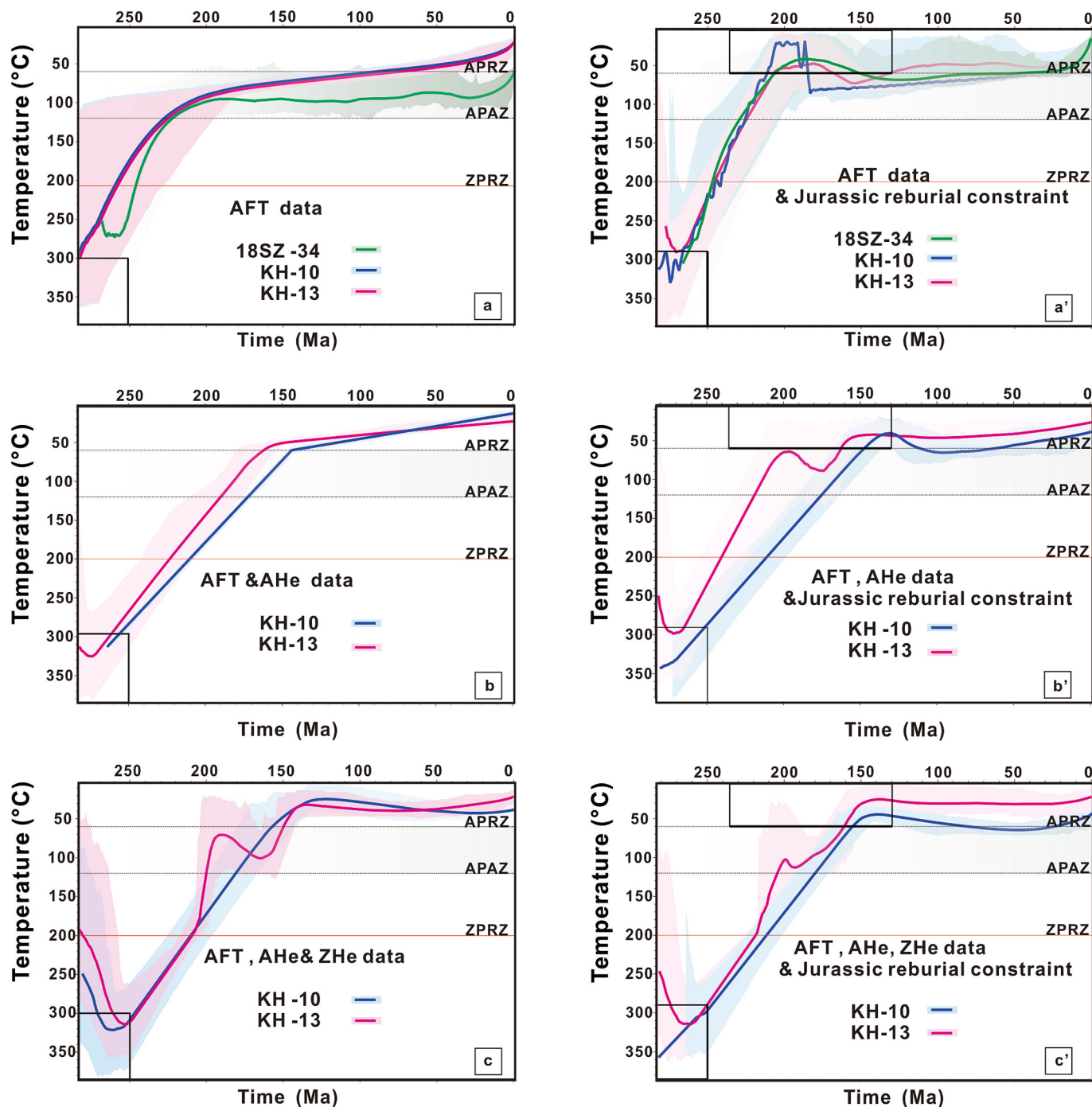


Fig. 7. QTQt thermal history inversion maps based on AFT, AHe, and ZHe data. Posterior probability distributions of accepted thermal history models are shown, with the solid line representing the expected (weighted mean) model and the shaded region showing the 95% confidence intervals. The black box in the lower left marks biotite Ar age, providing an additional thermal history constraint for the model's starting point. In models (a'-c'), reburial after uplift to the surface or near-surface during the Jurassic is included as an independent geological constraint (black box at the top), compared to unconstrained models (a-c).

2023; Wang et al., 2023). Conversely, northward regions experienced slower cooling and peneplanation since the Late Jurassic. Our samples and those from the Tuwu-Yandong indicate cooling rates of $< 1^{\circ}\text{C}/\text{Ma}$, corresponding to exhumation thicknesses of 1.2–2.3 km since the Late Cretaceous (Sun et al., 2021; He et al., 2022a).

5.2. The cooling of Qiziltag intrusion

Building on our analysis of controversial Mesozoic cooling events, we present a well-constrained thermal history for the Qiziltag intrusion.

This history begins with a zircon U-Pb age of 280–260 Ma and an amphibole Ar-Ar age of ~ 270 Ma (Fig. 8), providing the framework for reconstructing the evolution of cooling events.

The initial cooling phase (~ 290 to ~ 260 Ma) corresponds to the post-emplacement thermal relaxation of the pluton. Following pluton emplacement, the loss of heat from the original magma chamber led to thermal exchange with the surrounding country rock, resulting in a rapid cooling process. During this phase, temperatures decreased from at least 800°C to the closure temperature of biotite Ar-Ar ($\sim 350^{\circ}\text{C}$) by ~ 260 Ma, with cooling rates exceeding $20^{\circ}\text{C}/\text{Ma}$ and peaking near

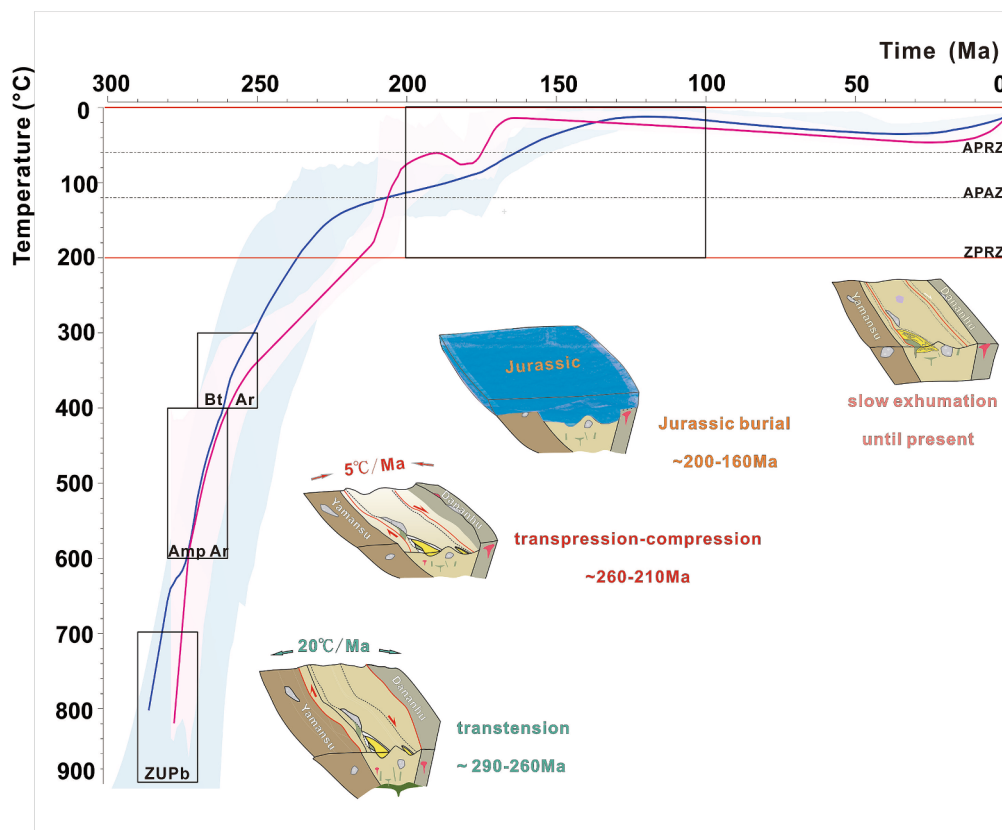


Fig. 8. Schematic diagrams depicting the uplift and denudation history of the Qiziltag pluton, based on integrated QTQt thermal history results for ZHe, AFT, and AHe, with additional constraints from ZUPb, AmpAr, and BtAr. See text for details.

75°C/Ma. Such rapid cooling is characteristic of post-magmatic processes and aligns with widespread extensional tectonics in the Eastern Tianshan. During this period, the region experienced peak rift evolution, with organic-rich sediments being extensively deposited (Zhang et al., 2019). Seismic data from the Turpan-Hami basin reveal Permian small-scale half-grabens and grabens, consistent with an extensional tectonic regime (Yang et al., 2010). This extensional environment is further supported by the presence of mantle-derived mafic–ultramafic rocks and bimodal intrusions in the area. Despite consensus on the extensional regime, the underlying tectonic drivers remain debated. Proposed mechanisms include the influence of the Permian Tarim mantle plume (Qin et al., 2011), the closure of the Paleo-Asian Ocean (Su et al., 2014), or ridge subduction processes (Feng et al., 2018). Each hypothesis reflects the complexity of the tectonic evolution during this time and highlights the need for integrated geophysical, petrological, and geochemical analyses to resolve these controversies (Branquet et al., 2012; Wang et al., 2014; Muhtar et al., 2019; Mao et al., 2022a).

The second cooling phase (~260 Ma onward) marks a major regional tectonic transition coinciding with the oblique collision between the Tarim craton and the southern CAOB (Ma et al., 1997; Xiao et al., 2018). Structural and geochronological evidence suggests a tectonic shift from transtension to compression (Laurent-Charvet et al., 2003; Hu et al., 2022; Mao et al., 2022a), initiating widespread intra-plate mountain building (De Grave et al., 2011; Glorie and De Grave, 2016). This transition is recorded in the regional stratigraphy by an unconformity where late Permian coarse-grained sediments rest unconformably atop middle Permian fine-grained deposits (Zhang et al., 2019). Basin provenance studies further support tectonic inversion from extension to compression by the middle-late Permian (Yang et al., 2009; Jiang et al., 2015). On a broader scale, this inversion reflects a tectonic regime change across the entire CAOB (Xiao et al., 2018).

Following this prolonged cooling phase, a minor burial event during

the Early-Middle Jurassic (~200 Ma to ~150 Ma) is evident in the thermal history. This event is consistent with stratigraphic data and reflects mild subsidence associated with Jurassic sediment deposition. Renewed cooling around ~150 Ma coincides with significant tectonic and climatic changes, potentially linked to the accretion of the Lhasa block along the southwestern margin of Eurasia (Hendrix et al., 1992; De Grave et al., 2014; Nachtergael et al., 2018) or regional aridification intensification (Shao et al., 2003). This cooling phase brought the Qiziltag intrusion to near-surface conditions. Subsequently, a prolonged period of slow cooling ensued, consistent with trends observed across the Tianshan mountain ranges (Morin et al., 2019). Unlike the southern Tianshan, where localized Cretaceous cooling events were more pronounced (Gillespie et al., 2017b), the Qiziltag region appears to have been relatively unaffected by such tectonic perturbations. This long-term stability is consistent with exhumation trends elsewhere in the range, reflecting subdued post-Jurassic tectonic activity.

5.3. Implication of exhumation and deposit preservation

The deformation patterns among different blocks in our study exhibit broad consistency, albeit with notable variations in exhumation intensity. By comparing the cooling histories of fault-bounded blocks, we emphasize that apparent ages – such as AFT and helium ages – serve as critical tools for regional exhumation comparisons rather than direct indicators of absolute cooling ages.

Since ~290 Ma, the study area has undergone intense tectonic activity driven by significant strike-slip faulting (Laurent-Charvet et al., 2002; Shu et al., 2002; Xu et al., 2003; Wang et al., 2014). While horizontal shearing was the dominant mechanism, vertical displacements also contributed significantly to the structural evolution. Initially, negative flower structures formed during the early exhumation phase, as indicated by older ZHe ages (250–230 Ma) in the Kanggur and Yamansu

belts (Figs. 8 and 9). In contrast, the Dananhu arc (220–180 Ma) and the Central Tianshan block (~210 Ma; Sun et al., 2021) experienced relatively younger ZHe ages, suggesting a more pronounced exhumation during this period. This phase of deformation transitioned into transpressional tectonics, forming positive flower structures with significant vertical displacements along the S-dipping Dacaotan fault (a branch of the Kanggur fault) and the N-dipping Aqikekuduk fault (Wang et al., 2008). These vertical displacements offset earlier structures, resulting in broadly consistent AFT ages within the margin of error across different blocks. During this phase, inherited structures facilitated moderate exhumation rates (~5 °C/Ma) in a contractional setting, bringing samples closer to the surface. The differential thickness of Jurassic strata, combined with paleogeographic factors and varying exhumation rates, resulted in a reburial effect during the Jurassic period. This burial phase was followed by renewed cooling, which brought samples back to near-surface conditions. The protracted cooling phase contributed to the progressive planation of late Paleozoic to early Mesozoic topographic relief, as described by Morin et al. (2019), leading to a uniform distribution of AHe ages across the region. Notably, the Yamansu belt exhibited distinctly younger AHe ages (Fig. 9), indicative of more intense denudation compared to the surrounding areas.

In the Chinese Tianshan orogen and adjacent Junggar region, porphyry and epithermal deposits, such as the Baogutu, Axi, and Yandong ore deposits, are located in low-altitude areas with older cooling ages (Gong et al., 2021). This spatial relationship between ore deposits and exhumation patterns is also evident in the Dananhu-Tousuquan belt, which hosts porphyry copper deposits, including the Tuwu-Yandong, Fuxing, Linglong and Yuhai deposits (Wang et al., 2016; Zhang et al., 2020a). These porphyry deposits typically form at depths of 1–6 km

(Sillitoe, 2010; Yanites and Kesler, 2015) and have been preserved due to limited exhumation and Jurassic reburial, which shielded them from subsequent erosion. The younger ZHe ages observed in this region suggest less exhumation compared to areas such as the Aqishan-Yamansu and Kanggur belts. Iron oxide copper-gold (IOCG)-like deposits, such as Heijianshan, Duotoushan, and Shuanglong in the Aqishan-Yamansu belt, share similar tectonic settings, host rocks, alteration styles, and mineralization processes. These deposits formed in an arc-related basin at depths of less than 5 km (Groves et al., 2021) and were preserved by the interplay of limited exhumation and Jurassic reburial (Han et al., 2019; Zhao et al., 2019; Zhang et al., 2023). The younger AHe ages in this belt further suggest that these samples are closer to the surface, enhancing their accessibility for geological surveys and mining.

Although detailed data, such as confined fission track length measurements, are currently insufficient to reconstruct the precise cooling history of the shear zone, some insights can still be drawn from the thermochronological ages. The similar ZHe and AFT ages observed across various sites, along with the older AHe ages compared to the Yamansu region, imply a relatively lower rate of exhumation since the Jurassic period. Volcanic rocks within this zone are characterized by their massive nature and the presence of amygdaloidal structures of varying sizes, which suggest crystallization occurred at shallow depths with minimal uplift and exhumation (Muhtar et al., 2022). As a result, this region has become an important locus for numerous epithermal gold deposits, such as Shiyingtan, Hongshi, and Kanggur (Wang et al., 2016; Muhtar et al., 2021).

Polymetallic metallogenic belts developed along the EW-trending shear zone in the Eastern Tianshan demonstrate contrasting

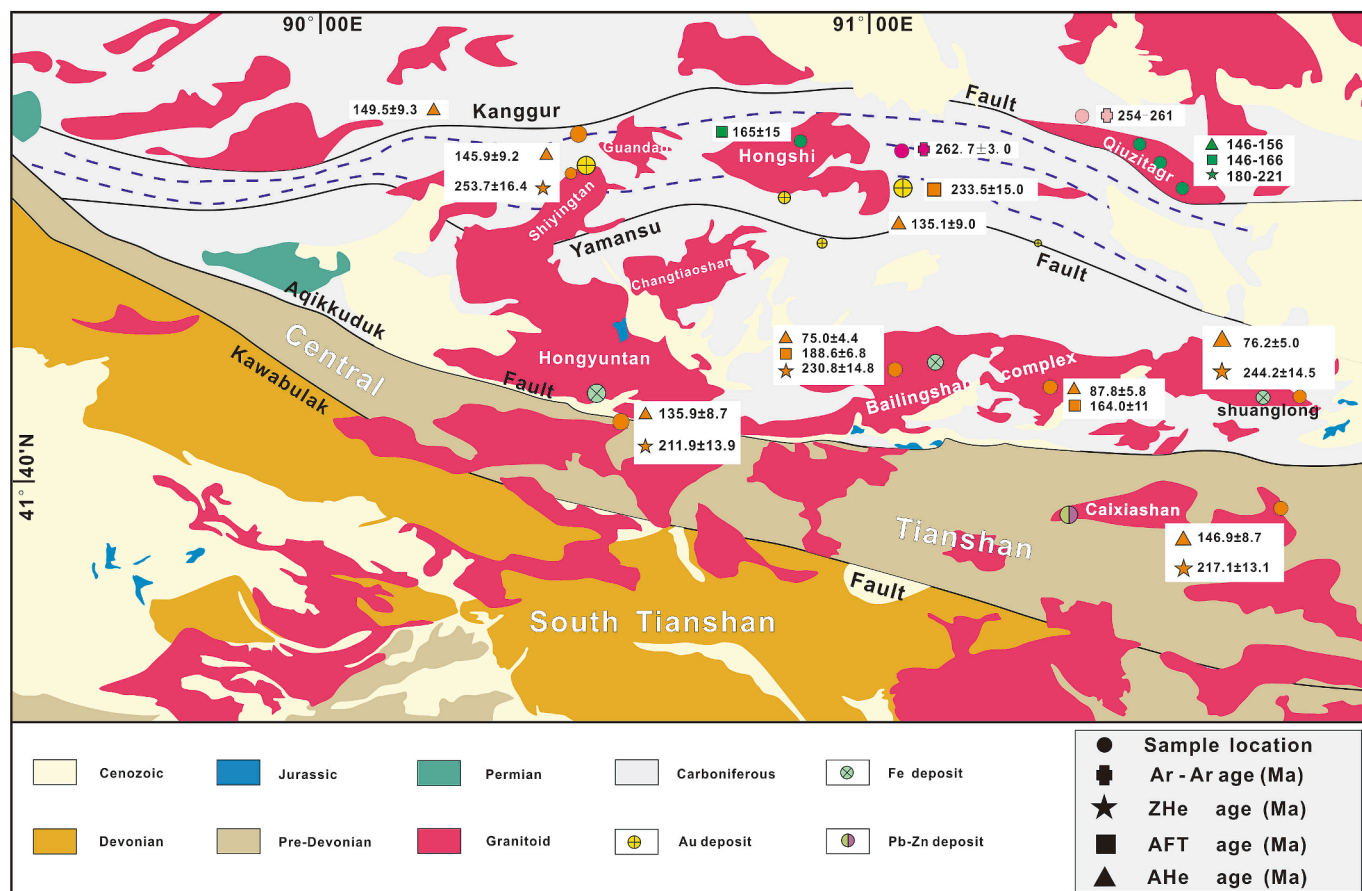


Fig. 9. Geological map of the western segment of the shear zone and adjacent areas (modified from Wang et al., 2006; Sun et al., 2021). Symbols: Ar/Ar – biotite sericite Ar/Ar ages; ZHe – zircon (U-Th)/He; AHe – apatite (U-Th)/He; AFT – apatite fission track. Sample locations are color-coded: orange (Sun et al., 2021), purple (Muhtar et al., 2022), pink (Wang et al., 2006), and green (this study).

exhumation patterns between its western and eastern parts, with significant implications for the types of deposits in these regions. The western part, which has undergone limited exhumation (Muhtar et al., 2022; Luo et al., 2023), is characterized by porphyry and epithermal deposits that typically form at shallower depths within the crust. In contrast, the eastern part has experienced more extensive cooling and exhumation, exposing magmatic Cu-Ni sulfide ore deposits, such as those at the Huangshan and Huangshandong (Wu et al., 2017), as well as the Tianyu and Baishiquan areas (Tang et al., 2011). These magmatic Cu-Ni sulfide deposits, which mineralized in the middle crust at depths of 11–15 km, were only brought to the surface through significant exhumation of the host rocks. This differential exhumation underscores the tectonic and thermal evolution of the shear zone and highlights its influence on the preservation and accessibility of mineral resources for mining and exploration.

6. Conclusion

Based on new findings and previously published data from the region, the following conclusions regarding the evolution of the western Kanggur-Huangshan ductile shear zone can be drawn:

(1) The Qiziltag intrusion was emplaced within a regional extensional setting between ~ 290 and ~ 266 Ma. Following post-magmatic cooling, it underwent moderate Triassic exhumation at a cooling rate of ~ 5 °C/Ma, closely associated with shear zone deformation. This cooling was subsequently impeded by Jurassic reburial, leading to renewed denudation in the Late Jurassic and a prolonged cooling period that ultimately brought the sample to the surface.

(2) Mesozoic cooling in the Eastern Tianshan was moderate and occurred in pulses. The presence of discrete blocks with varying thicknesses and differential paleotopography resulted in diverse degrees of cooling across the region.

(3) The combination of moderate Mesozoic exhumation, Jurassic reburial, and limited Cretaceous and Cenozoic exhumation suggests that the western part of the shear zone holds significant potential for polymetallic exploration.

CRediT authorship contribution statement

Meng Luo: Writing – original draft, Investigation, Formal analysis, Data curation. **Zhiyuan He:** Supervision, Funding acquisition, Formal analysis, Conceptualization, Writing – review & editing. **Fujun Wang:** Visualization, Investigation, Data curation, Writing – review & editing. **Yueqiao Zhang:** Writing – review & editing, Conceptualization. **Jianzhang Pang:** Writing – review & editing, Methodology. **Ying Wang:** Writing – review & editing, Methodology. **Ying Wu:** Writing – review & editing, Methodology. **Bihai Zheng:** Visualization, Data curation. **Johan De Grave:** Writing – review & editing. **Wenbin Zhu:** Supervision, Project administration, Funding acquisition, Writing – review & editing.

Declaration of competing interest

The authors declare that they have no known competing financial interests or personal relationships that could have appeared to influence the work reported in this paper.

Acknowledgements

This research was financially supported by the National Natural Science Foundation of China (NSFC-FWO bilateral project W2412032). Z. He is supported by an Alexander von Humboldt Research Fellowship for Postdocs in Germany. We are grateful to Shida Song (Ghent University) for his assistance in proofreading the manuscript. We thank Editor Prof. Michel Faure for his efficient editorial handling and two anonymous journal reviewers for their insightful reviews.

Appendix A. Supplementary data

Supplementary data to this article can be found online at <https://doi.org/10.1016/j.jseaes.2025.106560>.

Data availability

Data will be made available on request.

References

- Akciz, S.O., Burchfiel, B.C., Crowley, J.L., Yin, J.Y., Chen, L.Z., 2008. Geometry, kinematics and regional significance of the Chong Shan fault zone, east Himalayan syntaxis, Yunnan, China. *Geosphere* 4, 292–314.
- Ault, A.K., Gautheron, C., King, G.E., 2019. Innovations in (U-Th)/He, Fission Track, and Trapped Charge Thermochronometry with Applications to Earthquakes, Weathering, Surface-Mantle Connections, and the Growth and Decay of Mountains. *Tectonics* 38, 3705–3739.
- Barbarand, J., Carter, A., Wood, I., Hurford, T., 2003. Compositional and structural control of fission-track annealing in apatite. *Chemical Geology* 198 (1), 107–137.
- BGMRX (Bureau of Geology and Mineral Resources of Xinjiang), 1993. Regional Geology of Xinjiang Uygur Autonomous Region. Geological Publishing House, 1–841 (in Chinese).
- Branquet, Y., Gumiaux, C., Sizaret, S., Barbanson, L., Wang, B., Cluzel, D., Li, G.R., Delaunay, A., 2012. Synkinematic mafic/ultramafic sheeted intrusions: Emplacement mechanism and strain restoration of the Permian Huangshan Ni-Cu ore belt (Eastern Tianshan, NW China). *J Asian Earth Sci* 56, 240–257.
- Bullen, M.E., Burbank, D.W., Garver, J.I., Abdurakhmatov, K.Y., 2001. Late Cenozoic tectonic evolution of the northwestern Tien Shan: new age estimates for the initiation of mountain building. *Geol Soc Am Bull* 113, 1544–1559.
- Charvet, J., Shu, L.S., Laurent-Charvet, S., 2007. Paleozoic structural and geodynamic evolution of eastern Tianshan (NW China): welding of the Tarim and Junggar plates. *Episodes Journal of International Geoscience* 30, 162–186.
- Chen, K., Gumiaux, C., Augier, R., Chen, Y., Wang, Q.C., Lin, W., Wang, S.L., 2011. The Mesozoic palaeorelief of the northern Tian Shan (China). *Terra Nova* 23, 195–205.
- Chen, Y., Wang, G.C., Kapp, P., Shen, T.Y., Zhang, P., Zhu, C.Y., Cao, K., 2020. Episodic exhumation and related tectonic controlling during Mesozoic in the Eastern Tian Shan, Xinjiang, northwestern China. *Tectonophysics* 796, 228647.
- Cunningham, D., Owen, L., Snee, L., Li, J.L., 2003. Structural framework of a major intracontinental orogenic termination zone: The easternmost Tien Shan, China. *J Geol Soc* 160, 575–590.
- De Grave, J., Glorie, S., Buslov, M.M., Izmer, A., Fournier-Carrie, A., Batalev, V.Y., Vanhaecke, F., Elburg, M., Van den Haute, P., 2011. The thermo-tectonic history of the Song-Kul plateau, Kyrgyz Tien Shan: Constraints by apatite and titanite thermochronometry and zircon U/Pb dating. *Gondwana Res* 20 (4), 745–763.
- De Grave, J., De Pelsmaeker, E., Zhimulev, F.I., Glorie, S., Buslov, M.M., Van den Haute, P., 2014. Meso-Cenozoic building of the northern Central Asian Orogenic Belt: Thermotectonic history of the Tuva region. *Tectonophysics* 621, 44–59.
- Deng, X.H., Wang, J.B., Pirajno, F., Mao, Q.G., Long, L.L., 2020. A review of Cu-dominant mineral systems in the Kalatag district, East Tianshan, China. *Ore Geol Rev* 117, 103284.
- Du, L., Long, X.P., Yuan, C., Zhang, Y.Y., Huang, Z.Y., Wang, X.Y., Yang, Y.H., 2018. Mantle contribution and tectonic transition in the Aqishan-Yamansu Belt, Eastern Tianshan, NW China: Insights from geochronology and geochemistry of Early Carboniferous to Early Permian felsic intrusions. *Lithos* 304–307, 230–244.
- Dumitru, T.A., Zhou, D., Chang, E.Z., Graham, S.A., Carroll, A.R., 2001. Uplift, exhumation, and deformation in the Chinese Tian Shan. *Mem Geol Soc Am* 194, 71–99.
- Ehlers, T.A., Farley, K.A., 2003. Apatite (U-Th)/He thermochronometry: methods and applications to problems in tectonic and surface processes. *Earth Planet Sci Lett* 206, 1–14.
- Farley, K.A., Wolf, R.A., Silver, L.T., 1996. The effects of long alpha-stopping distances on (U-Th)/He ages. *Geochim Cosmochim Acta* 60, 4223–4229.
- Feng, Y.Q., Qian, Z.Z., Duan, J., Xu, G., Ren, M., Jiang, C., 2018. Geochronological and geochemical study of the Baixintan magmatic Ni-Cu sulphide deposit: New implications for the exploration potential in the western part of the East Tianshan nickel belt (NW China). *Ore Geol Rev* 95, 366–381.
- Flowers, R.M., Ketcham, R.A., Shuster, D.L., Farley, K.A., 2009. Apatite (U-Th)/He thermochronometry using a radiation damage accumulation and annealing model. *Geochim Cosmochim Acta* 73, 2347–2365.
- Gallagher, K., 2012. Transdimensional inverse thermal history modeling for quantitative thermochronology. *J Geophys Res Solid Earth* 117, 1–16.
- Gallagher, K., Charvin, K., Nielsen, S., Cambridge, M., Stephenson, J., 2009. Markov chain Monte Carlo (MCMC) sampling methods to determine optimal models, model resolution and model choice for Earth Science problems. *Mar Petrol Geol* 26 (4), 525–535.
- Gao, J., Gao, J., Klemd, R., Qian, Q., Zhang, X., Li, J.L., Jiang, T., Yang, Y.Q., 2011. The collision between the Yili and Tarim blocks of the Southwestern Altaids: Geochemical and age constraints of a leucogranite dike crosscutting the HP-LT metamorphic belt in the Chinese Tianshan Orogen. *Tectonophysics* 499, 118–131.
- Gillespie, J., Glorie, S., Jepson, G., Zhang, Z.Y., Xiao, W.J., Danišík, M., Collins, A.S., 2017a. Differential Exhumation and Crustal Tilting in the Easternmost Tianshan

- (Xinjiang, China), Revealed by Low-Temperature Thermochronology. *Tectonics* 36, 2142–2158.
- Gillespie, J., Glorie, S., Jepson, G., Zhang, Z.Y., Xiao, W.J., Danisik, M., Collins, A.S., 2017b. Mesozoic reactivation of the Beishan, southern Central Asian Orogenic Belt: Insights from low-temperature thermochronology. *Gondwana Res* 43, 107–122.
- Gillespie, J., Glorie, S., Jepson, G., Xiao, W.J., Collins, A.S., 2020. Late Paleozoic Exhumation of the West Junggar Mountains, NW China. *J Geophys Res Solid Earth* 125, e2019JB018013.
- Gleadow, A.J.W., Belton, D.X., Kohn, B.P., Brown, R.W., 2002a. Fission track dating of phosphate minerals and the thermochronology of apatite. *Rev Mineral Geochem* 48, 579–630.
- Gleadow, A.J.W., Kohn, B.P., Brown, R.W., O'Sullivan, P.B., Raza, A., 2002b. Fission track thermotectonic imaging of the Australian continent. *Tectonophysics* 349, 5–21.
- Glorie, S., De Grave, J., Buslov, M.M., Zhimulev, F.I., Stockli, D.F., Batalev, V.Y., Izmer, A., Haute, P.V.D., Vanhaecke, F., Elburg, M.A., 2011. Tectonic history of the Kyrgyz South Tien Shan (Atbashi-Inylchek) suture zone: the role of inherited structures during deformation-propagation. *Tectonics* 30, TC6016.
- Glorie, S., De Grave, J., 2016. Exhuming the Meso-Cenozoic Kyrgyz Tianshan and Siberian Altai-Sayan: A review based on low-temperature thermochronology. *Geosci Front* 7 (2), 155–170.
- Glorie, S., Jepson, G., Konopelko, D., Mirkamalov, R., Meeuws, F., Gilbert, S., Gillespie, J., Collins, A.S., Xiao, W., Dewaele, S., De Grave, J., 2019. Thermo-tectonic history of the Junggar Alatau within the Central Asian Orogenic Belt (SE Kazakhstan, NW China): insights from integrated apatite U/Pb, fission track and (UTh)/He thermochronology. *Geosci Front* 10, 2153–2166.
- Gong, L., Kohn, B., Zhang, Z.Y., Xiao, B., Wu, L., Chen, H.Y., 2021. Exhumation and Preservation of Paleozoic Porphyry Cu Deposits: Insights from the Yandong Deposit, Southern Central Asian Orogenic Belt. *Econ Geol* 116 (3), 607–628.
- Gong, L., Chen, H.Y., Wang, Q., Xiao, B., Zhang, S.L., Tang, G.J., 2023. Multiple tectonic switches in the Eastern Tianshan, Central Asian Orogenic Belt: Implications for crustal growth and metallogenesis. *Lithos* 454–455, 107235.
- Green, P.F., Duddy, I.R., Gleadow, A.J.W., Tingate, P.R., Laslett, G.M., 1986. Thermal annealing of fission tracks in apatite 1.A qualitative description. *Chem. Geol.* 59, 237–253.
- Groves, D.I., Condie, K.C., Goldfarb, R.J., Hronsky, J.M.A., Vielreicher, R.M., 2005. 100th Anniversary Special Paper: Secular Changes in Global Tectonic Processes and Their Influence on the Temporal Distribution of Gold-Bearing Mineral Deposits. *Econ Geol* 100, 203–224.
- Groves, D.I., Santosh, M., Zhang, L., Deng, J., Yang, L.Q., 2021. Subduction: The recycling engine room for global metallogeny. *Ore Geol Rev* 134, 104130.
- Guenther, W.R., Reiners, P.W., Ketcham, R.A., Nasdala, L., Giester, G., 2013. Helium diffusion in natural zircon: Radiation damage, anisotropy, and the interpretation of zircon (U-Th)/He thermochronology. *Am J Sci* 313, 145–198.
- Guenther, W.R., Reiners, P.W., Tian, Y.T., 2014. Interpreting date-eU correlations in zircon (U-Th)/He datasets: A case study from the Longmen Shan, China. *Earth Planet Sci Lett* 403, 328–339.
- Han, J.S., Chen, H.Y., Jiang, H.J., Zhao, L.D., Zhang, W.F., Lai, C.K., 2019. Genesis of the Paleozoic Aqishan-Yamansu arc-basin system and Fe (-Cu) mineralization in the Eastern Tianshan, NW China. *Ore Geol Rev* 105, 55–70.
- Han, B.F., He, G.Q., Wang, X.C., Guo, Z.J., 2011. Late Carboniferous collision between the Tarim and Kazakhstan-Yili terranes in the western segment of the South Tianshan Orogen, Central Asia, and implications for the Northern Xinjiang, western China. *Earth Sci Rev* 109 (3), 74–93.
- Han, C.M., Xiao, W.J., Wan, B., Ao, S.J., Zhang, J.E., Song, D.F., Zhang, Z.Y., Wang, Z.M., 2018. Late Palaeozoic-Mesozoic endogenetic metallogenic series and geodynamic evolution in the East Tianshan Mountains. *Acta Petrol Sin* 34, 1914–1932 in Chinese with English abstract.
- He, Z.Y., Wang, B., Nachtergaelie, S., Glorie, S., Ni, X.H., Su, W.B., Cai, D.X., Liu, J.S., De Grave, J., 2021a. Long-term topographic evolution of the Central Tianshan (NW China) constrained by low-temperature thermochronology. *Tectonophysics* 817, 229066.
- He, Z.Y., Wang, B., Ni, X.H., De Grave, J., Scaillet, S., Chen, Y., Liu, J.S., Zhu, X., 2021b. Structural and kinematic evolution of strike-slip shear zones around and in the Central Tianshan: insights for eastward tectonic wedging in the southwest Central Asian Orogenic Belt. *J Struct Geol* 144, 104279.
- He, Z.Y., Wang, B., Glorie, S., Ni, X.H., Liu, J.S., Cai, D.X., Zhong, L.L., De Grave, J., 2022b. Meso-Cenozoic thermo-tectonic evolution of the Yili block within the Central Asian Orogenic Belt (NW China): Insights from apatite fission track thermochronology. *Tectonophysics* 823, 229194.
- He, Z.Y., Glorie, S., Wang, F.J., Zhu, W.B., Fonseca, A., Su, W.B., Zhong, L.L., Zhu, X., De Grave, J., 2023a. A re-evaluation of the Meso-Cenozoic thermo-tectonic evolution of Bogda Shan (Tian Shan, NW China) based on new basement and detrital apatite fission track thermochronology. *Int Geol Rev* 65, 2093–2112.
- He, Z.Y., Zhong, L.L., Cao, K., Su, W.B., Glorie, S., Zhong, K.H., Sun, C., De Grave, J., 2023b. New constraints on the late oligocene-miocene thermo-tectonic evolution of the southeastern tibetan plateau from low-temperature thermochronology. *Tectonics* 42, e2023TC007881.
- Hendrix, M.S., 2000. Evolution of Mesozoic Sandstone Compositions, Southern Junggar, Northern Tarim, and Western Turpan Basins, Northwest China: A Detrital Record of the Ancestral Tian Shan. *J Sediment Res* 70, 520–532.
- Hendrix, M.S., Graham, S.A., Carroll, A.R., Sober, E.R., McKnight, C.L., Shulein, B.J., Wang, Z.X., 1992. Sedimentary record and climatic implications of recurrent deformation of the Tien Shan: evidence from Mesozoic strata of the North Tarim, South Junggar and Turpan basins. *Geol Soc Am Bull* 104, 53–79.
- Hu, A.Q., Wei, G.J., Zheng, J.B., Deng, W.F., Chen, L.L., 2007. SHRIMP U-Pb age for zircons of East Tianshan granitic gneiss and tectonic evolution significance from the eastern Tianshan Mountains, Xinjiang, China. *Acta Petrol Sin* 23 (8), 1795–1802 in Chinese with English abstract.
- Hu, J., Yu, X.Q., Zeng, Y., Lu, Z.Y., Wang, Z.F., 2022. Structural evolution of the Kanggur tectonic belt: implications for the latest carboniferous to Permian orogeny in the Eastern Tianshan, NW China. *Int Geol Rev* 64, 1670–1697.
- Huang, B., Fu, D., Kusky, T., Ruan, K.P., Zhou, W.X., Zhang, X.H., 2018. Sedimentary provenance in response to Carboniferous arc-basin evolution of East Junggar and North Tianshan belts in the southwestern Central Asian Orogenic Belt. *Tectonophysics* 722, 324–341.
- Jiang, S.H., Li, S.Z., Somerville, I.D., Lei, J.P., Yang, H.Y., 2015. Carboniferous-Permian tectonic evolution and sedimentation of the Turpan-Hami Basin, NW China: Implications for the closure of the Paleo-Asian Ocean. *J Asian Earth Sci* 113, 644–655.
- Jolivet, M., Dominguez, S., Charreau, J., Chen, Y., Li, Y.G., Wang, Q.C., Jolivet, C., 2010. Mesozoic and Cenozoic tectonic history of the Central Chinese Tian Shan: Reactivated tectonic structures and active deformation. *Tectonics* 29, TC6019.
- Ketcham, R.A., Carter, A., Donelick, R.A., Barbarand, J., Hurford, A.J., 2007. Improved modeling of fission-track annealing in apatite. *Am Mineral* 92, 799–810.
- Laurent-Charvet, S., Charvet, J., Shu, L.S., Ma, R.S., Lu, H.F., 2002. Paleozoic late collisional strike-slip deformations in Tianshan and Altay, Eastern Xinjiang, NW China. *Terra Nova* 14 (4), 249–256.
- Laurent-Charvet, S., Charvet, J., Monié, P., Shu, L.S., 2003. Late Paleozoic strike-slip shear zones in eastern central Asia (NW China): New structural and geochronological data. *Tectonics* 22 (2), 1009.
- Li, S.Z., Ren, Y., Feng, X.C., Li, S.L., 2006. Zircon SHRIMP U-Pb dating of granodiorite in the Kizil Tag composite intrusion, south margin of the Tufufan-Hami basin, East Tianshan, Xinjiang, China: With a discussion of the age of emplacement of the intrusion. *Geol Bull China* 25 (8), 937–940 in Chinese with English abstract.
- Li, Y.J., Zheng, D.W., Wu, Y., Wang, Y., He, H.Y., Pang, J.Z., Wang, Y.Z., Yu, J.X., 2017. A Potential (U-Th)/He Zircon Reference Material from Penglai Zircon Megacrysts. *Geostand Geoanalyt Res* 41, 359–365.
- Li, K., Chen, X.H., Zuza, A.V., Shao, Z.G., Qin, X., Han, L.L., Zhang, Y.P., Yu, W., Wang, Z.Z., Shi, X.B., Li, B., Wang, Y., 2023. The Late Mesozoic Intracontinental contraction-Extension Transition in the Beishan Fold-Thrust Belt, Central Asia: Constraints From Structural Analysis and Apatite (U-Th)/He Thermochronology. *Tectonics* 42 (7), e2022TC007532.
- Liu, Y.G., Lü, X.B., Wu, C.M., Hu, X.G., Duan, Z.P., Deng, G., Wang, H., Zhu, X.K., Zeng, H.D., Wang, P., 2016. The migration of Tarim plume magma toward the northeast in Early Permian and its significance for the exploration of PGE-Cu-Ni magmatic sulfide deposits in Xinjiang, NW China: As suggested by Sr-Nd-Hf isotopes, sedimentology and geophysical data. *Ore Geol Rev* 538–545.
- Luo, M., He, Z.Y., Wang, F.J., Zhu, W.B., Li, G.W., De Grave, J., Wang, Y.Q., Zheng, B.H., Zhang, Y.Q., 2023. Exhumation and preservation of the Tianyu Cu-Ni deposit constrained by low-temperature thermochronology: Insights into the thermo-tectonic history of the Chinese Eastern Tianshan. *Ore Geol Rev* 154, 105309.
- Ma, R.S., Shu, L.S., Sun, J., 1997. Tectonic evolution and metallogeny of Eastern Tianshan mountains. Geological Publishing House.
- Macaulay, E.A., Sobel, E.R., Mikolaichuk, A., Kohn, B., Stuart, F.M., 2014. Cenozoic deformation and exhumation history of the Central Kyrgyz Tien Shan. *Tectonics* 33, 135–165.
- Mao, Q.G., Xiao, W.J., Windley, B.F., Yu, M.J., Zhang, J.E., 2019. Early Permian subduction-related transtension in the Turpan Basin, East Tianshan (NW China): implications for accretionary tectonics of the southern Altaiids. *Geol Mag* 1–24.
- Mao, Q.G., Ao, S.J., Windley, B.F., Zhang, Z.Y., Song, D.F., Zhang, J.E., Wan, B., Tan, W., Han, C.M., Xiao, W.F., 2021. Petrogenesis of Late Carboniferous-Early Permian mafic-ultramafic-felsic complexes in the eastern Central Tianshan, NW China: The result of subduction-related transtension? *Gondwana Res* 95, 72–87.
- Mao, Q.G., Xiao, W.J., Buckman, S., Huang, P., Ao, S.J., Song, D.F., Zhang, J.E., Sang, Miao, S., Tan, Z., Wang, H., Li, R., 2022a. Deformational History of the Kanguer Subduction Complex in the Eastern Tianshan (NW China): Implications for Paleozoic-Triassic Multiple Accretionary Tectonics of the Southern Altaiids. *Tectonics* 41(11), e2022TC007527.
- Mao, Q.G., Xiao, W.J., Buckman, S., Huang, P., Ao, S.J., Song, D.F., Zhang, J.E., Sang, M., Tan, Z., Wang, H., Li, R., 2022b. Middle-Late Triassic southward-younging granitoids: Tectonic transition from subduction to collision in the Eastern Tianshan-Beishan Orogen, NW China. *Geol Soc Am Bull* 134, 2206–2224.
- Molnar, P., Tapponnier, P., 1975. Cenozoic Tectonics of Asia: Effects of a Continental Collision. *Science* 189, 419–426.
- Morin, J., Jolivet, M., Barrière, L., Laborde, A., Li, H.B., Dauteuil, O., 2019. Planation surfaces of the Tian Shan Range (Central Asia): Insight on several 100 million years of topographic evolution. *J Asian Earth Sci* 177, 52–65.
- Muhtar, M.N., Wu, C.Z., Santosh, M., Lei, R.X., Gu, L.X., Wang, S.M., Gan, K., 2019. Late Paleozoic tectonic transition from subduction to post-collisional extension in Eastern Tianshan, Central Asian Orogenic Belt. *Geol Soc Am Bull* 132, 1756–1774.
- Muhtar, M.N., Wu, C.Z., Brzozowski, M.J., Lei, R.X., Feng, Z.J., Chen, B.Y., Jiang, Y.H., 2021. Sericitic 40Ar/39Ar dating and S-Pb isotope composition of the Kanggur gold deposit: Implications for metallogenesis of late Paleozoic gold deposits in the Tianshan, central Asian Orogenic Belt. *Ore Geol Rev* 131, 104056.
- Muhtar, M.N., Wu, C.Z., Matthew, J.B., Santosh, M., Tian, R.S., Xie, G.A., Zhang, W.F., Lei, R.X., Xiao, W.J., 2022. Timing and spatial variation of deformation along the Kanggur-Huangshan shear zone in the Chinese Tianshan: Implications for regional differential uplift and mineralization. *Geol Soc Am Bull* 135, 1429–1448.

- Nachtergaelie, S., De Pelsmaeker, E., Glorie, S., Zhimulev, F., Jolivet, M., Danišk, M., Buslov, M.M., De Grave, J., 2018. Meso-Cenozoic tectonic evolution of the Tals-Fergana region of the Kyrgyz Tian Shan revealed by low-temperature basement and detrital thermochronology. *Geosci Front* 9, 1495–1514.
- Oriolo, S., Wemmer, K., Oyhantçabal, P., Fosse, H., Schulz, B., Siegesmund, S., 2018. Geochronology of shear zones-A review. *Earth Sci Rev* 185, 665–683.
- Pang, J.Z., Zheng, D.W., Ma, Y., Wang, Y., Wu, Y., Wan, J.L., Yu, J.X., Li, Y.J., Wang, Y.Z., 2017. Combined apatite fission-track dating, chlorine and REE content analysis by LA-ICPMS. *Sci Bull* 62, 1497–1500.
- Passchier, C.W., Trouw, R.A.J., 2005. Microtectonics. Springer-Verlag, Berlin.
- Paton, C., Woodhead, J.D., Hellstrom, J.C., Hergt, J.M., Greig, A., Maas, R., 2010. Improved laser ablation U-Pb zircon geochronology through robust downhole fractionation correction. *Geochim Geophys Geosys* 11 (3), 1–36.
- Qin, K.Z., Su, B.X., Sakyl, P.A., Tang, D.M., Li, X.H., Sun, H., Xiao, Q.H., Liu, P.P., 2011. Sims zircon U-Pb geochronology and sr-nd isotopes of ni-cu-bearing mafic-ultramafic intrusions in eastern tianshan and beishan in correlation with flood basalts in tarim basin (nw china): constraints on a ca. 280 Ma mantle plume. *Am J Sci* 311, 237–260.
- Reiners, P.W., Spell, T.L., Niculescu, S., Zanetti, K.A., 2004. Zircon (U-Th)/He thermochronometry: He diffusion and comparisons with 40 Ar/ 39 Ar dating. *Geochim Cosmochim Acta* 68, 1857–1887.
- Reinoso, F., Marquardt, M., Cembrano, J., Pérez-Flores, P., Díaz-Alvarado, J., Folguera, A., 2024. Tectonic setting, structures, and Au-Cu mineralization age of the Indiana deposit: An example of ore deposit formation controlled by Andean transverse faults, Atacama region. *Chile. J South Am Earth Sci* 133, 104705.
- Ribeiro, B.V., Mulder, J.A., Faleiros, F.M., Kirkland, C.L., Cawood, P.A., O'Sullivan, G., Campanha, G.A.C., Finch, M.A., Weinberg, R.F., Nebel, O., 2020. Using apatite to resolve the age and protoliths of mid-crustal shear zones: A case study from the Taxaquara Shear Zone, SE Brazil. *Lithos* 378–379.
- Sengör, A.M.C., Natal'in, B.A., Burtman, V.S., 1993. Evolution of the Altai tectonic collage and Palaeozoic crustal growth in Eurasia. *Nature* 364, 299–307.
- Shao, L.Y., Zhang, P.F., Hilton, J., Gayer, R., Wang, Y.B., Zhao, C.Y., Luo, Z., 2003. Paleoenvironment and paleogeography of the Lower and lower Middle Jurassic coal measures in the Turpan-Hami oil-prone coal basin, northwestern China. *AAPG Bulletin* 87 (2), 335–355.
- Shu, L.S., Charvet, J., Lu, H.F., Laurent-Charvet, S., 2002. Paleozoic accretion-collision events and kinematics of ductile deformation in the central-southern Tianshan Belt, China. *Acta Geol Sin* 76, 308–323.
- Sillitoe, R.H., 2010. Porphyry Copper Systems. *Econ Geol* 105, 3–41.
- Sobel, E.R., 1999. Basin analysis of the Jurassic-Lower Cretaceous southwest Tarim basin, northwest China. *Geol Soc Am Bull* 111, 709–724.
- Sobel, E.R., Chen, J., Heerman, R.V., 2006. Late Oligocene-Early Miocene initiation of shortening in the Southwestern Chinese Tian Shan: Implications for Neogene shortening rate variations. *Earth Planet Sci Lett* 247, 70–81.
- Song, S.D., Li, J.G., Liu, X.Y., Wang, Y.D., Liang, W.T., Yuan, S.H., 2023. Mesozoic-Cenozoic Exhumation History of the Bogda Range, Eastern Tianshan: Insights from Apatite Fission Track Thermochronology. *Minerals* 13 (1), 71.
- Su, B.X., Qin, K.Z., Zhou, M.F., Sakyl, P., Thakurta, J., Tang, D.M., Liu, P.P., Xiao, Q.H., Sun, H., 2014. Petrological, geochemical and geochronological constraints on the origin of the Xiadong Ural-Alaskan type complex in NW China and tectonic implication for the evolution of southern Central Asian Orogenic Belt. *Lithos* 200–201, 226–240.
- Sun, M., Lin, S.Y., Zhang, F.F., Wang, Y.H., Xue, C.J., Zhang, T.T., Guo, J.W., Wen, X.Y., 2021. Post-ore change and preservation of the late Paleozoic Tuwu porphyry Cu deposit in Eastern Tianshan, NW China: Constraints from geology and apatite fission track thermochronology. *Ore Geol Rev* 137, 104297.
- Sun, J.B., Sun, T.F., Chen, W., Yu, S., Yin, J.Y., Li, C., Zhang, Y., Liu, X.Y., 2015. Thermo-tectonic evolution history of Hongyuntan area, eastern Tianshan, Xinjiang: constrained from Ar-Ar and (U-Th)/He dating. *Acta Petrol Sin* 31, 3732–3742 in Chinese with English abstract.
- Tang, D.M., Qin, K.Z., Li, C.S., Qi, L., Su, B.X., Qu, W.J., 2011. Zircon dating, Hf-Sr-Nd-O isotopes and PGE geochemistry of the Tianyu sulfide-bearing mafic-ultramafic intrusion in the Central Asian Orogenic Belt, NW China. *Lithos* 126, 84–98.
- Vermeesch, P., 2009. RadialPlotter: A Java application for fission track, luminescence and other radial plots. *Radiation Measurements* 44 (4), 409–410.
- Vernon, R.H., 2004. A Practical Guide to Rock Microstructure. Cambridge University Press.
- Wang, Y.N., Cai, K.D., Sun, M., Xiao, W.J., De Grave, J., Wan, B., Bao, Z.H., 2018b. Tracking the multi-stage exhumation history of the western Chinese Tianshan by Apatite Fission Track (AFT) dating: Implications for the preservation of epithermal deposits in the ancient orogenic belt. *Ore Geol Rev* 100, 111–132.
- Wang, B., Cluzel, D., Jahn, B.M., Shu, L.S., Chen, Y., Zhai, Y.Z., Brunquet, Y., Barbanson, L., Sizaret, S., 2014. Late Paleozoic pre- and syn-kinematic plutons of the Kangguer-Huangshan Shear zone: Inference on the tectonic evolution of the eastern Chinese north Tianshan. *Am J Sci* 314, 43–79.
- Wang, F.J., Luo, M., He, Z.Y., Ge, R.F., Cao, Y.Y., De Grave, J., Zhu, W.B., 2022. Late Mesozoic intracontinental deformation and magmatism in the Chinese Tianshan and adjacent areas. *Central Asia. GSA Bulletin* 134 (11–12), 3003–3021.
- Wang, F.J., Luo, M., He, Z.Y., Zheng, B.H., Zhang, Z.Y., Hu, X., Zhu, W.B., 2023. Mid-Cretaceous Accelerated Cooling of the Beishan Orogen, NW China: Evidence from Apatite Fission Track Thermochronology. *Lithosphere* 14, lithosphere_2023_239.
- Wang, F.J., He, Z.Y., Ge, R.F., Luo, M., Zheng, B.H., Zhang, Z.Y., Tian, R.S., Cao, Y.Y., Zhu, W.B., 2024. First identification of late Mesozoic intraplate magmatism in the Chinese north Tianshan: implications for the orogenic architecture and crustal evolution. *Journal of the Geological Society* 181, jgs2023-176.
- Wang, K., Ji, W.H., Meng, Y., Zhang, X., Zhu, X.H., Li, P., 2019. Deformation in Eastern Tianshan Orogenic Belt: Response to the Final Stage of Accretionary Orogenesis. *Geotecton Metall* 43, 894–910.
- Wang, Y., Li, J.Y., Sun, G.H., 2008. Postcollisional Eastward Extrusion and Tectonic Exhumation along the Eastern Tianshan Orogen, Central Asia: Constraints from Dextral Strike-Slip Motion and 40Ar/39Ar Geochronological Evidence. *J Geol* 116, 599–618.
- Wang, C.Y., Ma, R.S., Shu, L.S., Zhu, W.B., 1994. Study on the regional metamorphism and the tectonic wettings in the eastern Tianshan orogenic belt. *J Nanjing Univ (natural Science Edition)* 30, 494–503 in Chinese with English abstract.
- Wang, J.F., Shu, L.S., 1997. A study of ultramicro structure of quartz in the ductile shear zones in the Tianshan belt, Xinjiang. *J Nanjing Univ: Nat Sci Ed* 33, 464–470 in Chinese with English abstract.
- Wang, J.B., Wang, Y.W., He, Z.J., 2006. Ore deposits as a guide to the tectonic evolution in the East Tianshan Mountains, NW China. *Geol Chin* 33, 461–469 in Chinese with English abstract.
- Wang, Y.H., Xue, C.J., Gao, J.B., Zhang, F.F., Liu, J.J., Wang, J.P., Wang, J.C., 2016a. The genesis of the ores and granitic rocks at the Hongshi Au deposit in Eastern Tianshan, China: Constraints from zircon U-Pb geochronology, geochemistry and isotope systematics. *Ore Geol Rev* 74, 122–138.
- Wang, B., Zhai, Y.Z., Kapp, P., De Jong, K., Zhong, L.L., Liu, H.S., Ma, Y.Z., Gong, H.J., Geng, H.Y., 2018a. Accretionary tectonics of back-arc oceanic basins in the South Tianshan: Insights from structural, geochronological, and geochemical studies of the Wuwamen ophiolite mélange. *Geol Soc Am Bull* 130, 284–306.
- Wang, Y.H., Zhang, F.F., Liu, J.J., 2016b. The genesis of the ores and intrusions at the Yuhai Cu-Mo deposit in eastern Tianshan, NW China: Constraints from geology, geochronology, geochemistry, and Hf isotope systematics. *Ore Geol Rev* 77, 312–331.
- Windley, B.F., Alexeev, D., Xiao, W.J., Krone, A., Badarch, G., 2007. Tectonic models for accretion of the Central Asian Orogenic Belt. *J Geo Soc* 164, 31–47.
- Wu, C.Z., Xie, S.W., Gu, L.X., Samson, I.M., Yang, T., Lei, R.X., Zhu, Z.Y., Dang, B., 2017. Shear zone-controlled post-magmatic ore formation in the Huangshandong Ni-Cu sulfide deposit, NW China. *Ore Geol Rev* 100, 545–560.
- Xiao, W.J., Windley, B., Hao, J., Zhai, M.G., 2003. Accretion leading to collision and the Permian Solonker suture, Inner Mongolia, China: termination of the central Asian orogenetic belt. *Tectonics* 22, 1069–1088.
- Xiao, W.J., Zhang, L.C., Qin, K.Z., Sun, S., Li, J.L., 2004. Paleozoic accretionary and collisional tectonics of the eastern Tianshan (China): implications for the continental growth of central Asia. *Am J Sci* 304, 370–395.
- Xiao, W.J., Windley, B.E., Allen, M.B., Han, C.M., 2013. Paleozoic multiple accretionary and collisional tectonics of the Chinese Tianshan orogenic collage. *Gondwana Res* 23, 1316–1341.
- Xiao, W.J., Windley, B.F., Han, C.M., Liu, W., Wan, B., Zhang, J.E., Ao, S.J., Zhang, Z.Y., Song, D.F., 2018. Late Paleozoic to early Triassic multiple roll-back and oroclinal bending of the Mongolia collage in Central Asia. *Earth-Sci Rev* 186, 94–128.
- Xiao, W.J., Liu, Y.J., Somerville, I., Schulmann, K., Kusky, T., Seltmann, R., 2020. Accretionary tectonics, deep structures and metallogeny of southern Altaids. *Geol J* 55, 1613–1619.
- Xu, X.W., Ma, T.L., Sun, L.Q., Cai, X.P., 2003. Characteristics and dynamic origin of the large-scale Jiaoluotuo ductile compressional zone in the eastern Tianshan Mountains, China. *J Struct Geol* 25, 1901–1915.
- Yang, W., Feng, Q., Liu, Y.Q., Tabor, N., Miggins, D., Crowley, J.L., Lin, J.Y., Thomas, S., 2010. Depositional environments and cyclo-and chronostratigraphy of uppermost Carboniferous-Lower Triassic fluvial-lacustrine deposits, southern Bogda Mountains, NW China—A terrestrial paleoclimatic record of mid-latitude NE Pangea. *Glob Planet Chan* 73, 15–113.
- Yang, Y.T., Guo, Z.X., Song, C.C., Li, X.B., He, S., 2015. A short-lived but significant Mongol-Okhotsk collisional orogeny in latest Jurassic-earliest Cretaceous. *Gondwana Res* 28, 1096–1116.
- Yang, T.N., Li, J.Y., Wang, Y., Dang, Y.X., 2009. Late Early Permian (266 Ma) N-S compressional deformation of the Turfan basin, NW China: the cause of the change in basin pattern. *Int J Earth Sci* 98 (6), 1311–1324.
- Yanites, B.J., Kesler, S.E., 2015. A climate signal in exhumation patterns revealed by porphyry copper deposits. *Nature Geosci* 8, 462–465.
- Yin, J.Y., Chen, W., Thomson, S.N., Sun, M., Wang, Y.N., Xiao, W.J., Yuan, C., Sun, J.B., Long, X.P., 2019. Fission track thermochronology of the Tuwu-Yandong porphyry Cu deposits, NW China: Constraints on preservation and exhumation. *Ore Geol Rev* 113, 103104.
- Yin, J.Y., Wang, Y.N., Hodges, K.V., Xiao, W.J., Thomson, S.N., Chen, W., Yuan, C., Sun, M., Cai, K.D., Sun, J.B., 2023. Episodic Long-Term Exhumation of the Tianshan Orogenic Belt: New Insights From Multiple Low-Temperature Thermochronometers. *Tectonics* 42, e2022TC007469.
- Zhai, Y.S., Deng, J., Peng, R.M., 2000. Research contents and methods for post-ore changes, modifications and preservation. *Earth Sci-J China Univ Geosci* 340–345 in Chinese with English abstract.
- Zhang, S.L., Chen, H.Y., Hollings, P., Zhao, L.D., Gong, L., 2020b. Tectonic and magmatic evolution of the Aqishan-Yamansu belt: A Paleozoic arc-related basin in the Eastern Tianshan (NW China). *Geol Soc Am Bull* 133 (5–6), 1320–1344.
- Zhang, S.L., Chen, H.Y., Xiao, B., Zhao, L.D., Hu, X., Li, J.P., Gong, L., 2023. Textural and chemical evolution of magnetite from the Paleozoic Shuanglong Fe-Cu deposit: Implications for tracing ore-forming fluids. *Am Mineral* 108, 178–191.
- Zhang, J., Cunningham, D., 2012. Kilometer-scale refolded folds caused by strike-slip reversal and intraplate shortening in the Beishan region, China. *Tectonics* 31, TC3009.

- Zhang, Y.Y., Sun, M., Yuan, C., Long, X.P., Jiang, Y.D., Li, P.F., Huang, Z.Y., Du, L., 2018. Alternating Trench Advance and Retreat: Insights From Paleozoic Magmatism in the Eastern Tianshan, Central Asian Orogenic Belt. *Tectonics* 37, 2142–2164.
- Zhang, S.H., Wang, J.Q., Liu, C.Y., Bai, J.K., Peng, H., Huang, H.X., Guan, Y.Z., 2019. Detrital zircon U-Pb geochronology of the Permian strata in the Turpan-Hami Basin in North Xinjiang, NW China: Depositional age, provenance, and tectonic implications. *Geol Journal* 54 (2), 1064–1080.
- Zhang, W., Zhang, F.F., Wang, Y.H., Xue, C.J., Wang, J.P., Sun, M., Wang, K., 2020a. Origin of Paleozoic granitoids in the Yuhai Cu-Mo deposit, Eastern Tianshan, NW China and implications for regional metallogeny. *Ore Geol Rev* 121, 103465.
- Zhang, X.R., Zhao, G.C., Eizenhöfer, P.R., Sun, M., Han, Y.G., Hou, W.Z., Liu, D.X., Wang, B., Liu, Q., Xu, B., 2015. Paleozoic magmatism and metamorphism in the Central Tianshan block revealed by U-Pb and Lu-Hf isotope studies of detrital zircons from the South Tianshan belt, NW China. *Lithos* 233, 193–208.
- Zhang, X.R., Zhao, G.C., Sun, M., Eizenhöfer, P.R., Han, Y.G., Hou, W.Z., Liu, D.X., Wang, B., Liu, Q., Xu, B., 2016. Tectonic evolution from subduction to arc-continent collision of the Junggar ocean: Constraints from U-Pb dating and Hf isotopes of detrital zircons from the North Tianshan belt, NW China. *Geol Soc Am Bull* 128, 644–660.
- Zhang, D.Y., Zhou, T.F., Yuan, F., Fan, Y., Deng, Y.F., Xu, C., Zhang, R.F., 2014. Genesis of Permian granites along the Kangguer Shear Zone, Jueluotage area, Northwest China: Geological and geochemical evidence. *Lithos* 198–199, 141–152.
- Zhao, L.D., Chen, H.Y., Hollings, P., Han, J.S., 2019. Late Paleozoic magmatism and metallogenesis in the Aqishan-Yamansu belt, Eastern Tianshan: Constraints from the Bailingshan intrusive complex. *Gondwana Res* 65, 68–85.
- Zheng, Y., Zhang, Q., Wang, Y., Liu, R., Wang, S.G., Zuo, G., Wang, S.Z., Lkaasuren, B., Badarch, G., Badamgarav, Z., 1996. Great Jurassic thrust sheets in Beishan (north Mountains)—Gobi areas of China and southern Mongolia. *J Struct Geol* 18, 1111–1126.
- Zhong, L.L., Wang, B., De Jong, K., Zhai, Y.Z., Liu, H.S., 2019. Deformed continental arc sequences in the South Tianshan: New constraints on the Early Paleozoic accretionary tectonics of the Central Asian Orogenic Belt. *Tectonophysics* 768, 228169.
- Zhou, T.F., Yuan, F., Zhang, D.Y., Fan, Y., Liu, S., Peng, M.X., Zhang, J.D., 2010. Geochronology, tectonic setting and mineralization of granitoids in Jueluotage area, eastern Tianshan, Xinjiang. *Acta Petrol Sinica* 26, 478–502 in Chinese with English abstract.